General Disclaimer

One or more of the Following Statements may affect this Document

- This document has been reproduced from the best copy furnished by the organizational source. It is being released in the interest of making available as much information as possible.

- This document may contain data, which exceeds the sheet parameters. It was furnished in this condition by the organizational source and is the best copy available.

- This document may contain tone-on-tone or color graphs, charts and/or pictures, which have been reproduced in black and white.

- This document is paginated as submitted by the original source.

- Portions of this document are not fully legible due to the historical nature of some of the material. However, it is the best reproduction available from the original submission.

NASA CR-168051
PWA-5768-29

NASA

MODEL AERODYNAMIC TEST RESULTS FOR A REFINED ACTUATED INLET EJECTOR NOZZLE AT SIMULATED TAKEOFF AND CRUISE CONDITIONS FINAL REPORT

by

D.P. Nelson

June 1983

UNITED TECHNOLOGIES CORPORATION
Pratt & Whitney Aircraft Group
Commercial Engineering

Prepared for

NATIONAL AERONAUTICS AND SPACE ADMINISTRATION
NASA-Lewis Research Center
Contract NAS3-22738

1. REPORT NO. NASA CR-168051	2. GOVERNMENT AGENCY	3. RECIPIENT'S CATALOG NO.
4. TITLE AND SUBTITLE Model Aerodynamic Test Results for a Refined Actuated Inlet Ejector Nozzle at Simulated Takeoff and Cruise Conditions - Final Report		5. REPORT DATE June 1983 6. PERFORMING ORG. CODE
7. AUTHOR(S) D. P. Nelson		8. PERFORMING ORG. REPT. NO. PWA-5768-29
9. PERFORMING ORG. NAME AND ADDRESS United Technologies Corporation Pratt & Whitney Aircraft Group Commercial Engineering		10. WORK UNIT NO. 11. CONTRACT OR GRANT NO. NAS3-22738
12. SPONSORING AGENCY NAME AND ADDRESS National Aeronautics and Space Administration 21000 Brookpark Road Cleveland, Ohio 44135		13. TYPE REPT./PERIOD COVERED Contractor Final Report 14. SPONSORING AGENCY CODE

15. SUPPLEMENTARY NOTES

NASA Technical Manager: Mr. Donald L. Bresnahan

16. ABSTRACT

Wind tunnel model tests were conducted to demonstrate the aerodynamic performance improvements of a refined actuated inlet ejector nozzle. Models of approximately one-tenth scale were configured to simulate nozzle operation at takeoff, subsonic cruise, transonic cruise and supersonic cruise. Variations of model components provided a performance evaluation of ejector inlet and exit area, forebody boattail angle and ejector inlet operation in the open and closed mode.

Approximately 700 data points were acquired at Mach numbers of 0, 0.36, 0.9, 1.2, and 2.0 for a wide range of nozzle flow conditions. Results show that relative to two ejector nozzles previously tested performance was improved significantly at takeoff and subsonic cruise. Takeoff quiescent and fly-over performance was improved 0.3 and 1.6 percent respectively. At subsonic cruise a 4.2 percent improvement was demonstrated. Good supersonic cruise performance, a C_f of 0.982, was attained equal to the high performance of the previous tests. The established advanced supersonic transport propulsion study performance goals were met or closely approached at takeoff and supersonic cruise. Subsonic cruise performance was within 2.3 percent of the target. Analysis of the data show that further improvements are possible. Although a transonic cruise performance goal has not been established, results were less than desired, with a C_f of 0.866. Analysis of the data show that performance improvements are possible.

17. KEY WORDS (SUGGESTED BY AUTHOR(S))	18. DISTRIBUTION STATEMENT
Coannular Exhaust Nozzle, Actuated Inlet Ejector, Advanced Supersonic Propulsion System	To be distributed to U.S. Government Agencies and their contractors only

19. SECURITY CLASS (THIS REPT)	20. SECURITY CLASS (THIS PAGE)	21. NO. PGS	22. PRICE *
Unclassified	Unclassified	76	

* For sale by the National Technical Information Service, Springfield, VA 22161

TABLE OF CONTENTS

LIST OF FIGURES

LIST OF FIGURES (Cont'd)

LIST OF FIGURES (Cont'd)

LIST OF FIGURES (Cont'd)

LIST OF TABLES

SECTION 1.0

SUMMARY

This report presents the results of a wind tunnel test program conducted to demonstrate the aerodynamic performance improvements of a refined actuated inlet ejector nozzle. The nozzle models were tested at takeoff, subsonic cruise, and supersonic cruise conditions and performance was also checked at transonic cruise. This work concludes the experimental and analytical design study programs conducted by Pratt & Whitney Aircraft, under NASA sponsorship, to develop the coannular nozzle technology required for a high thrust performance, low jet noise exhaust system for an Advanced Supersonic Transport (AST) propulsion system.

Wind tunnel performance tests were performed using scale models of a refined, variable-geometry ejector nozzle. Design refinements to the previously tested actuated inlet ejector exhaust system included replacing the ejector shroud clam shell with a hinged shroud flap and modifying the fan duct nozzle with a long hinged flap. The primary nozzle flowpath was also revised. The refined design retained the high radius ratio fan nozzle feature for low jet noise. Five basic models of approximately one-tenth scale (21.6 cm, 8.5 in.) diameter were fabricated and tested in the NASA-Lewis 8 by 6 Foot Supersonic Wind Tunnel. The models simulated nozzle operation at takeoff, subsonic cruise, transonic cruise, and supersonic cruise. Each configuration was instrumented with 39 surface static pressure taps.

Approximately 700 data points were acquired at test Mach numbers of 0, 0.36, 0.9, 1.2, and 2.0 for a wide range of nozzle flow conditions. Aerodynamic test variables included fan nozzle pressure ratio and fan-to-primary total pressure split commensurate with engine operation at each flight condition. Geometric variables included ejector shroud inlet and exit area for the takeoff and subsonic cruise models. Forebody boattail angle was also varied for the subsonic cruise configuration. Transonic cruise model variables included shroud geometries simulating ejector inlet open and closed operation. Fan and primary nozzle areas were varied to match engine operating conditions.

Comparisons with the previously tested ejector nozzles show a significant improvement in takeoff and subsonic cruise thrust coefficients (C_f). At takeoff quiescent and fly-over conditions, thrust coefficient was improved 0.3 and 1.6 percent, respectively. At subsonic cruise, a 4.2 percent improvement was demonstrated. Good supersonic cruise performance, a C_f of 0.982, was measured, equal to the high levels of the previous tests. The results show the established AST propulsion study performance goals were met or closely approached at takeoff conditions, and the goal was achieved at supersonic cruise. Subsonic cruise performance was within 2.3 percent of the target. Analysis of the data show further improvements are possible.

Performance maps of varying ejector inlet and exit area showed that the maximum quiescent takeoff performance, C_f = 0.983, was obtained with the

largest inlet and smallest exit area tested. Maximum fly-over performance, C_f = 0.974, occurred over a range of large inlet areas and the minimum exit area. Maximum subsonic cruise performance, C_f = 0.917, was observed at the minimum inlet and exit areas tested. These subsonic results were obtained with the minimum forebody boattail angle tested; increasing boattail angle resulted in decreased performance.

Although a transonic cruise performance goal was not established, results were less than desired with a C_f = 0.866. Comparison of results with the ejector configured in the open and closed mode showed the mode of operation had little effect on nozzle performance at the engine operating conditions. Static pressure tap data indicate excessive inlet flow separation, and internal shock losses were responsible for the unsatisfactory performance of the inlet open ejector configuration. The similar level of performance for the ejector closed configuration is attributed to large internal nozzle over-expansion losses. The analysis showed that improved performance is possible with design modifications to eliminate inlet flow separation and minimize shock losses.

SECTION 2.0

INTRODUCTION

2.1 BACKGROUND

Pratt & Whitney Aircraft has been participating in a series of NASA-sponsored programs aimed at establishing a propulsion system technology base for an Advanced Supersonic Cruise Transport (AST). A major result has been the identification and refinement of the Variable Stream Control Engine (VSCE) (ref. 1) as a promising approach to the economic and environmental requirements of the propulsion system.

This system, an advanced turbofan engine, is characterized by two critical technology components: a low emissions duct burner and a variable geometry coannular nozzle to achieve low fuel consumption and low jet noise. To develop the technology for the nozzle exhaust system, several aerodynamic and acoustic analytical studies and experimental model tests were conducted under the NASA Coannular Nozzle Technology Program (ref. 2, 3, and 4).

As part of this effort, the thrust performance of two potential ejector nozzles had been evaluated in a series of wind tunnel tests (ref. 5). Nozzle performance goals were achieved for the critical supersonic flight mode, but not for takeoff or subsonic cruise. Several mechanical and aerodynamic design refinements have since been incorporated (ref. 6) to correct these deficiencies without compromising the good supersonic performance already demonstrated.

The primary objectives of the current effort was to verify the performance improvements of these refinements at takeoff and subsonic cruise and to confirm a high level of performance at supersonic cruise. A secondary objective was to check performance at transonic cruise, a flight regime that recent airframe studies (ref. 7) indicated may be attractive.

2.2 PROGRAM DESCRIPTION

Five basic 0.103 scale models of the refined ejector nozzle were fabricated to simulate the variable-geometry nozzle operation at takeoff, subsonic cruise, transonic cruise (ejector shroud inlet open and closed), and supersonic cruise. Model performance tests were conducted in the NASA-Lewis 8x6 Foot Supersonic Wind Tunnel.

Approximately 700 data points were acquired for variations of the five models at Mach numbers of 0, 0.36, 0.9, 1.2, and 2.0 for a wide range of nozzle flow conditions. Variations of the coannular nozzle operating conditions included fan duct nozzle pressure ratio and fan-to-primary total pressure split commensurate with VSCE operating conditions at each flight Mach number. Geometric variables included ejector shroud inlet and exit area for the takeoff and subsonic cruise configurations. Forebody boattail angle was also

varied for the subsonic cruise models. Transonic cruise configuration variables included shroud geometries that simulated ejector inlet operation in the open and closed mode. Fan and primary nozzle areas were varied to match engine requirements for each flight condition.

Tests were also conducted with a modified Supersonic Tunnel Association nozzle to verify the facility thrust and flow measuring systems.

Nozzle charging station pressure, temperature, and weight flow were measured for each stream along with nozzle generated thrust. Results in terms of thrust and flow coefficient formed the basis for the data analyses. Model surface static pressures were also measured and analyzed to provide an understanding of the performance trends. The results of the test program are presented in this report. Detailed data in tabular and graphical form are presented under separate cover in the companion Comprehensive Data Report (ref. 8).

SECTION 3.0

FACILITY AND TEST EQUIPMENT

3.1 TEST FACILITY

The test program was conducted in the NASA Lewis 8 by 6 Foot Supersonic Wind Tunnel (ref. 9). The research test nozzles were attached to a 21.59 cm (8.5 in.) diameter cylindrical jet exit strut model supported in the test section by a perpendicular strut connected to the tunnel ceiling, shown in Figures 3.1-1 and 3.1-2. Air was supplied through long, flexible tubes running down the strut into coannular air passages to the test nozzle. The air supply tubes were fixed to the tunnel ceiling at the top, which was nonmetric (forces here were not transmitted to the load cell), and to the coannular air passages at the bottom. Air flow from the tubes entered the coannular passages normal to the model centerline, thus eliminating any entering axial momentum force on the load cell. Static pressure instrumentation was located on the internal unstream facing surfaces of the metric hardware to account for tare forces that result when internal static pressures were different from ambient.

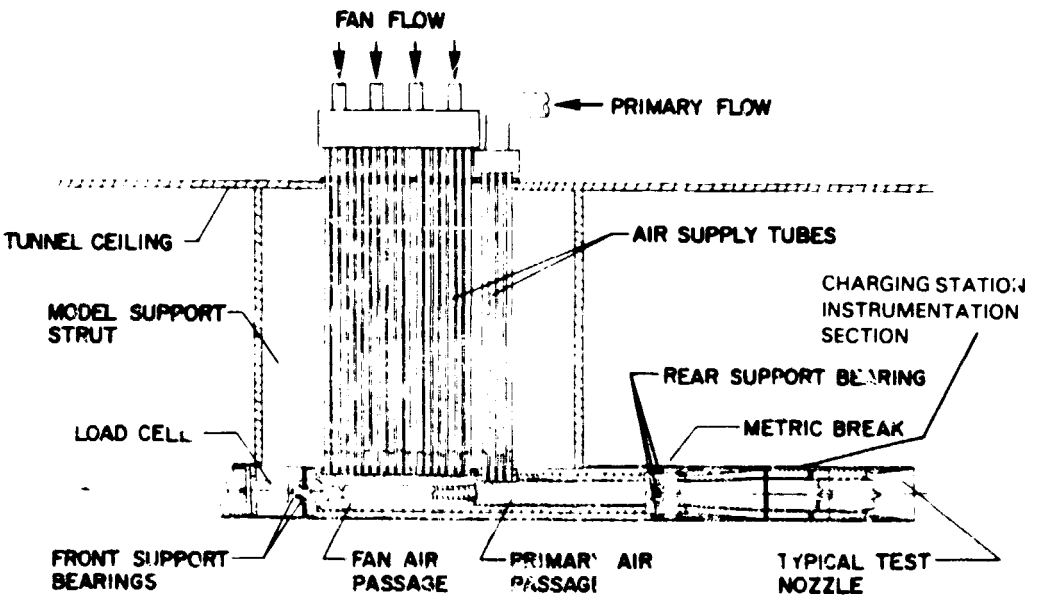

Figure 3.1-1 Diagram of Model Installed on The Jet Exit Strut in Wind Tunnel

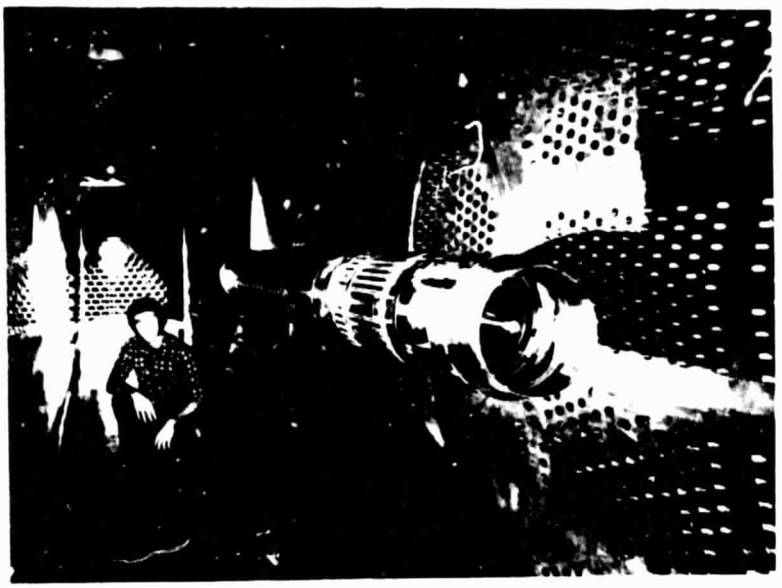

Figure 3.1-2 Typical Research Model Installed in NASA Lewis 8x6-Foot Supersonic Wind Tunnel

Nozzle thrust was measured with a load cell mounted in the forward portion of the model. The coannular air passages, supported by bearings at the front and rear, made contact with the load cell and were metric, i.e., axial forces acting on the model support coannular piping were measured by the load cell. The load cell was calibrated by applying a known axial force along the centerline of the model. This force was generated with a hydraulic cylinder connected to the model with the shaft of the cylinder pushing along the thrust axis of the nozzle. Correlation of the known applied force and the electrical output of the load cell provided the desired calibration from 0 to 8896 newtons (200 lbf), the maximum allowable balance load.

The air supply system is shown schematically in Figure 3.1-3. A compressor provided a continuous supply of air at 310 N/cm^2 (450 lbf/in.^{2} gage). The air, after passing through a gas-fired heat exchanger, flowed through a system of control valves and a flow meter and into the tubes within the model strut. As tunnel temperature increased with increasing freestream Mach number, up to a total temperature of 366K (200°F) at M_0 2.0, the model air supply was heated to reduce internal model temperature gradients. Over the range of test conditions up to M_0 1.2, the air supply was heated to 311K (100°F). At M_0 2.0 the air supply temperature was maintained at 327K (130°F).

Primary nozzle air was metered with a choked venturi, which had a 3.2995 cm (1.2990 in.) throat diameter. Fan nozzle air supply was metered through either a 4.4392 cm (1.7477 in.) or a 3.3058 cm (1.3015 in.) diameter choked venturi, depending on the flow rate required.

Tests were also conducted with a modified Supersonic Tunnel Association nozzle to verify the facility thrust and flow measuring systems. The results of these tests are described in Appendix A.

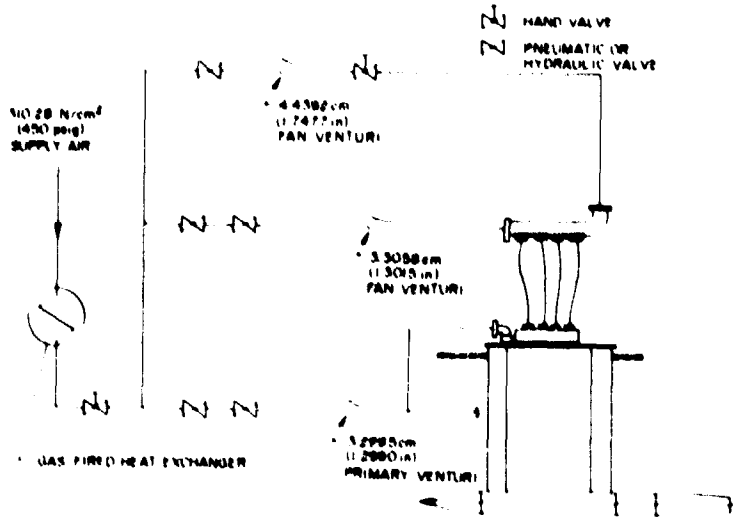

Figure 3.1-3 Model Air Supply System

3.2 EXHAUST SYSTEM DESIGN

The improved actuated inlet ejector design, Figure 3.2-1, is a result of several distinct refinements (ref. 6) specifically aimed at improving takeoff and subsonic cruise performance. The refined design incorporates a long hinged flap mechanism for fan duct stream flow control. An axially translatable centerbody plug provides primary stream control to satisfy the wide range of flow conditions of the VSCE 515 engine (ref. 1). Axially translating ejector inlet doors, designed to stow in the shroud, uncover the inlet to admit external flow as required in the takeoff through transonic flight regime. To establish the inlet flowpath, these doors act in conjunction with a set of internal hinged shroud flaps that pivot outward to the shroud leading edge and complete the external air flowpath to the ejector nozzle. In the inlet open operating mode, the actuated fan duct nozzle forms the upstream portion (forebody boattail) of the inlet flowpath. The actuated fan nozzle was designed to form a smooth continuous elliptical boattail (14° mean angle at subsonic cruise) to improve ejector inlet flow effectiveness and reduce boattail losses. Although transonic climb performance was a design consideration, the configuration was not designed to maximize performance at transonic cruise. Subsequent interest in transonic cruise operation (ref. 7) led to an evaluation of the design at this condition.

Predicted nozzle operating conditions for the VSCE 515 engine are shown in Table 3.2-I for the four flight conditions of interest. The operating conditions were defined on the basis of optimum installed engine performance. Airframe supplied inlet characteristics were utilized in the performance studies.

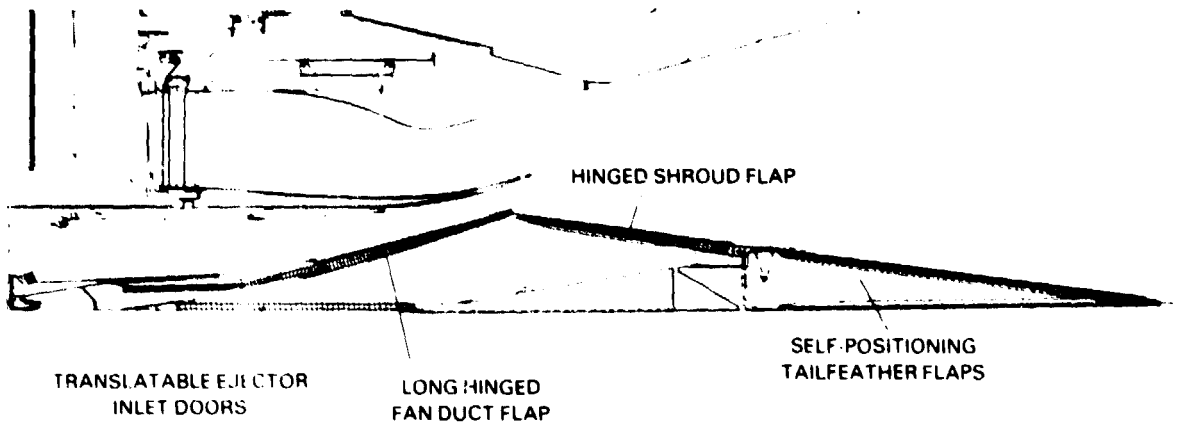

Figure 3.2-1 Actuated Inlet Ejector Nozzle Design

TABLE 3.2-I

VSCE 515 Operating Characteristics

Flight Condition	Fan Nozzle Pressure Ratio P_{tf}/P_o	Fan-to-Primary Total Pressure Split P_{tf}/P_{tp}
Takeoff	2.84	1.78
Subsonic Cruise	5.09	2.05
Transonic Cruise	7.31	1.35
Supersonic Cruise	27.6	2.12

3.2.1 Nozzle Model Configurations

Five basic 0.103-scale research model configurations of the refined actuated inlet ejector nozzle were provided for testing along with variations of the model components. The maximum diameter of the models was 21.6 cm (8.5 in.). The configurations were designed to simulate the variable nozzle geometry operating with the ejector inlet open at takeoff and subsonic cruise, both open and closed at transonic cruise, and closed at supersonic cruise. The nominal research model configuration for each operating mode and the variation of the model components are illustrated in Figure 3.2-2. The nozzle design parameters and component test variables, identified in Figure 3.2-2a and e, are tabulated in Table 3.2-II. The model component assemblies were designed such that the flow splitter remains fixed in position for all configurations. The relative positions of the centerbody plug, forebody boattail, ejector shroud leading edge, and exit area were varied to provide the individual configurations.

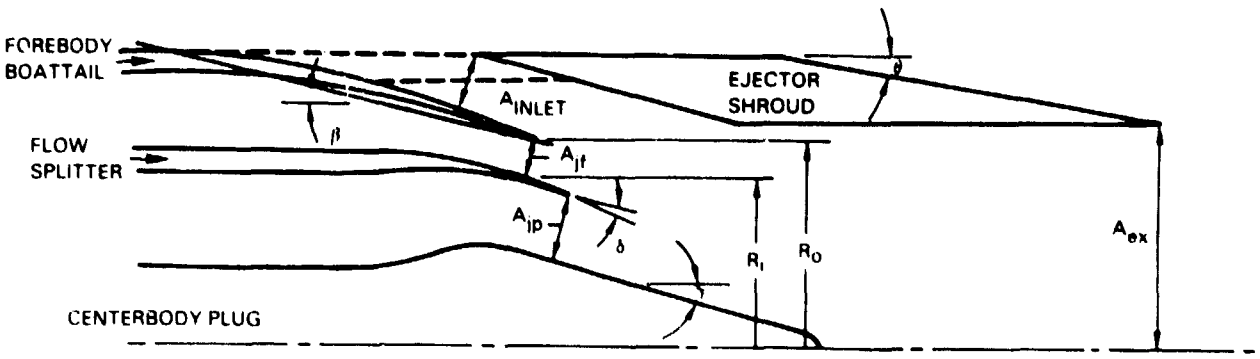

(a) Takeoff Configuration

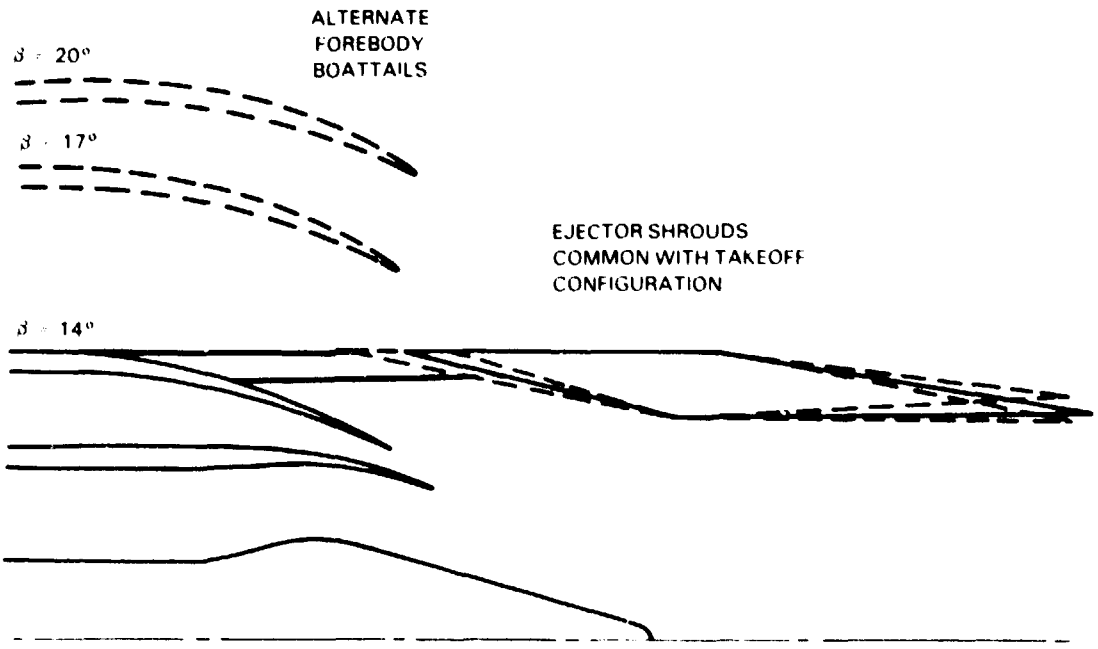

(b) Subsonic Cruise Configuration

Figure 3.2-2 Actuated Inlet Ejector Nozzle Configurations

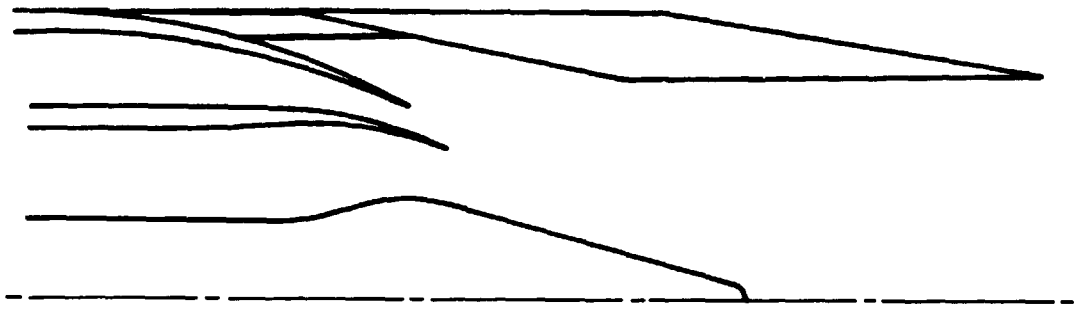

(c) Transonic Cruise - Ejector Open Configuraton

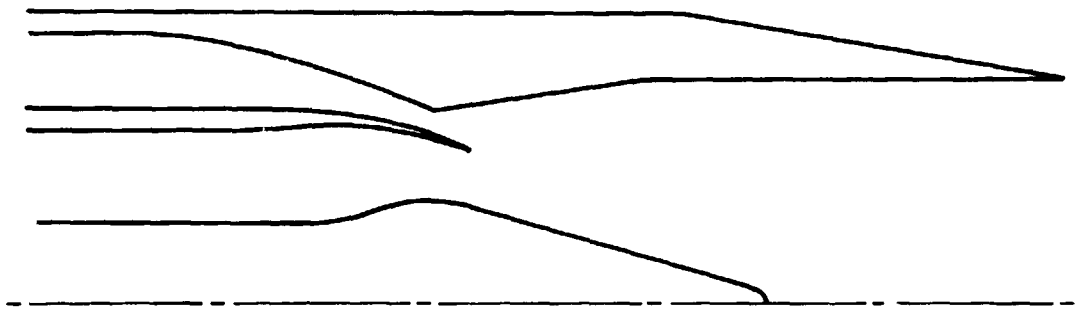

(d) Transonic Cruise - Ejector Inlet Closed Configuration

Figure 3.2-2 Actuated Inlet Ejector Nozzle Configurations (Continued)

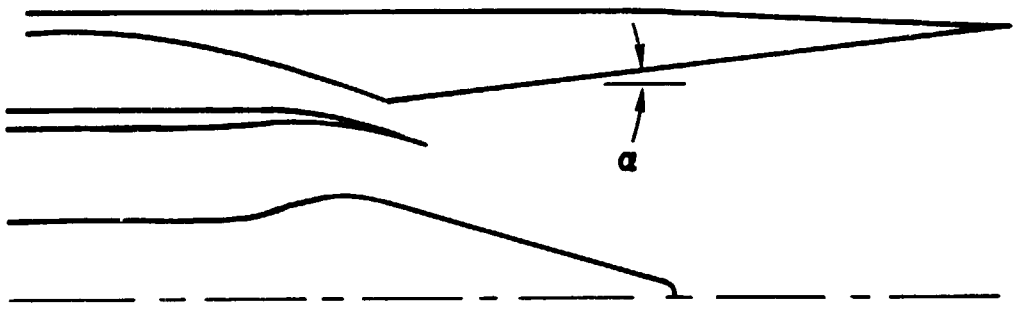

(e) Supersonic Cruise Configuation

Figure 3.2-2 Actuated Inlet Ejector Nozzle Configurations (Concluded)

Six interchangeable ejector shrouds, used in conjunction with strut spacers, provided the independent variation of ejector inlet and exit area for the takeoff and subsonic cruise configurations. Variation of the transonic cruise ejector inlet area was achieved with a separate shroud and strut spacers. Variation of the subsonic cruise forebody geometry was accomplished with three interchangeable forebodies of varying boattail angle. Two solid shrouds simulated the transonic and supersonic cruise ejector closed configurations. These shrouds also simulated the appropriate fan nozzle flowpaths. Photographs of a subsonic and supersonic cruise model assembly are shown in Figure 3.2-3. Prior to testing, the fastener access slots, seen in the figure, were filled with a mixture of talcum powder and dope and faired smooth with the original surface.

The models were fabricated primarily of 304 stainless steel. The assembly components were constructed to facilitate the interchange of similar items. The models were assembled to the jet exit strut instrumentation section (see Figure 3.1-1) described in the following section.

TABLE 3.2-II

Principal Nozzle Design Parameters (Model Scale)
(Reference Figure 3.2-2a & e)

Parameter	Configuration			
	Takeoff	Subsonic Cruise	Transonic Cruise	Supersonic Cruise
Primary Nozzle Area - A_{jp} cm^2 (in^2)	68.19 (10.570)	74.52 (11.550)	58.26 (9.031)	68.19 (10.570)
Fan Nozzle Area - A_{jf} cm^2 (in^2)	61.26 (9.495)	34.13 (5.290)	38.96 (6.039)	44.12 (6.839)
Ejector Exit Area Ratio ($A_{ex}/(A_{jp}+A_{jf})$)	1.60, 1.71, 1.88*	1.90, 2.04, 2.24*	2.28	2.95
Ejector Inlet Area Ratio ($A_{inlet}/A_{jp} + A_{jf}$))	0.67 to 0.87*	0.72 to 1.19*	0.63 to 0.75*	--
Forebody Boattail Angle (Degrees) - β	11.7	14, 17, 20*	13.5	--
Trailing Edge Flap Boattail Angle (Degrees) - θ	8.9	8.9	8.9	1.9
Shroud Internal Divergence Angle (Degrees) - α	--	--	--	6.7
Flow Impingement Angle (Degrees) - δ	5	5	5	5
Plug Half - Angle (Degrees) - γ	15	15	15	15
Fan Nozzle Radius Ratio (R_i/R_o)	0.831	--	--	--

* Test Variable

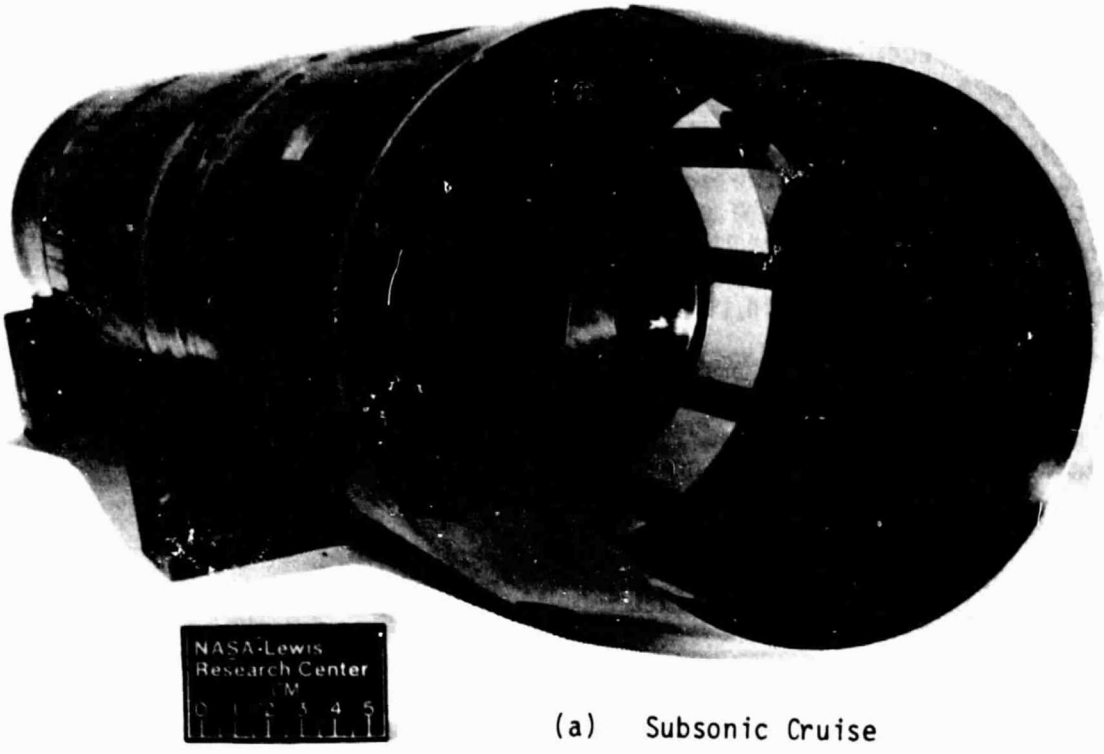

(a) Subsonic Cruise

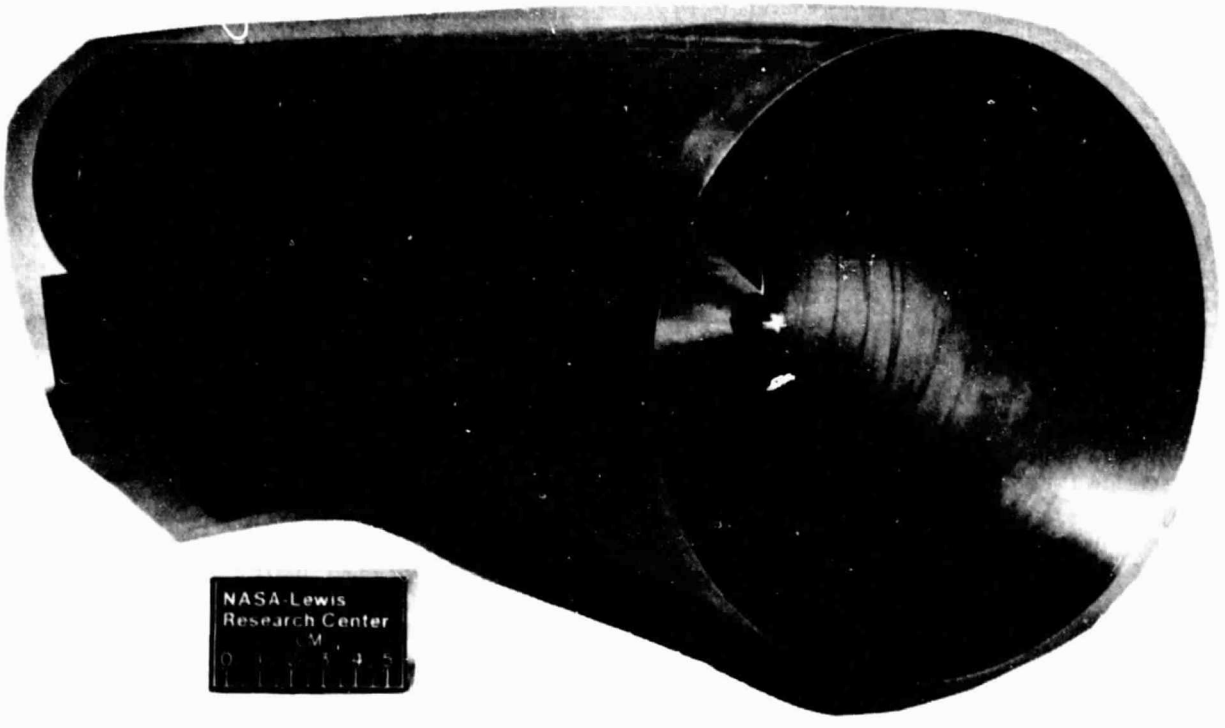

(b) Supersonic Cruise

Figure 3.2-3 Model Assemblies

3.2.2 Model Instrumentation

Fan and primary nozzle flow properties were defined by utilizing the charging station pressure and temperature instrumentation located upstream of the model in the jet exit strut instrumentation section. The section also contained flow conditioning choke plates and screens to provide uniform flow profiles at the charging station, as illustrated in Figure 3.2-4. The primary stream flow properties were measured with seven total pressure probes and three total temperature probes. Fan stream properties were measured with ten total pressure and three total temperature probes. Details of the instrumentation arrangement are described in reference 5.

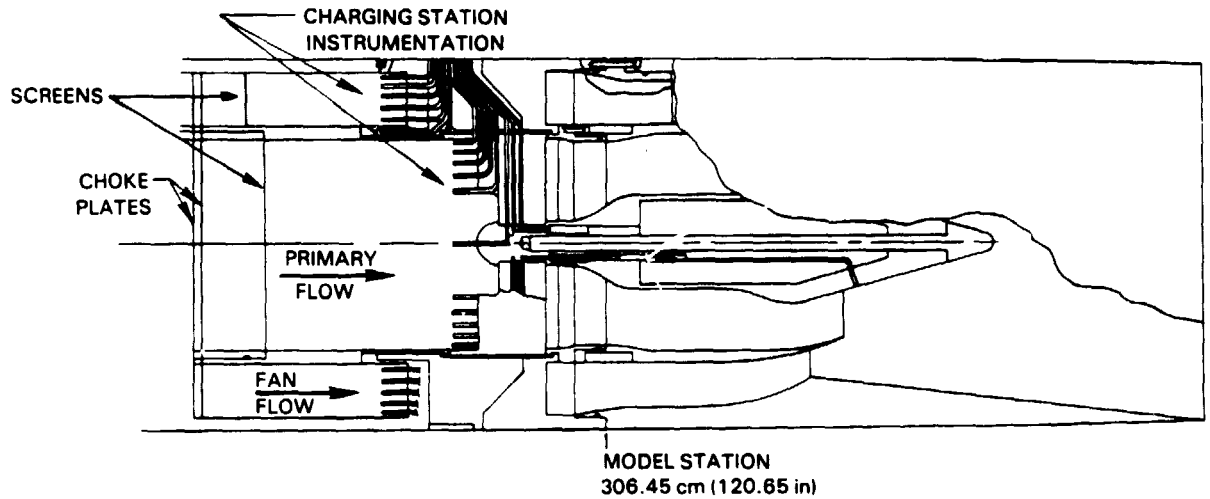

Figure 3.2-4 Model Charging Station Instrumentation

Each model configuration was instrumented with thirty-nine surface static pressure taps to aid in the analysis of the performance data. Static taps were installed on each model component with the majority concentrated on the forebody boattail and the ejector shroud. The instrumentation for each configuration is illustrated in Figure 3.2-5, a through e, and tabulated in Table 3.2-III. The tablular values of axial tap location ($X/D_{max.}$) are referenced relative to the forebody model connection flange (station 306.45 cm (120.65 in.)) and are normalized by the maximum model diameter, 21.59 cm (8.5 in.). During the test program, not all of the pressure data were recorded in some instances. The instrumentation is described to indicate what information is available.

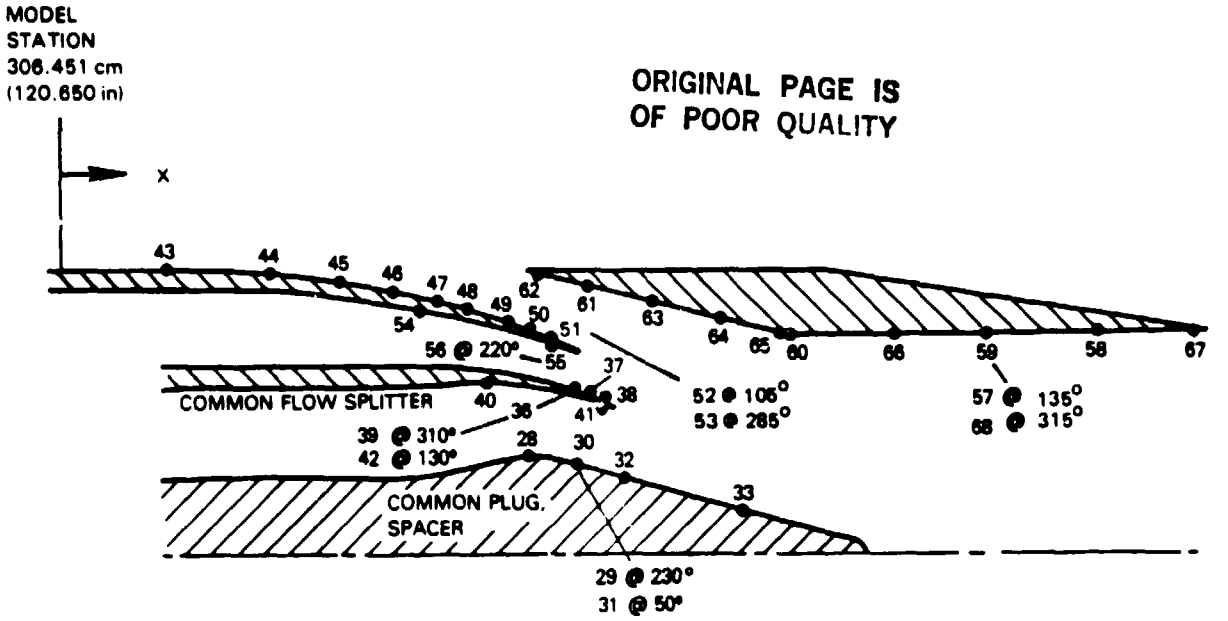

(a) Takeoff Configuration

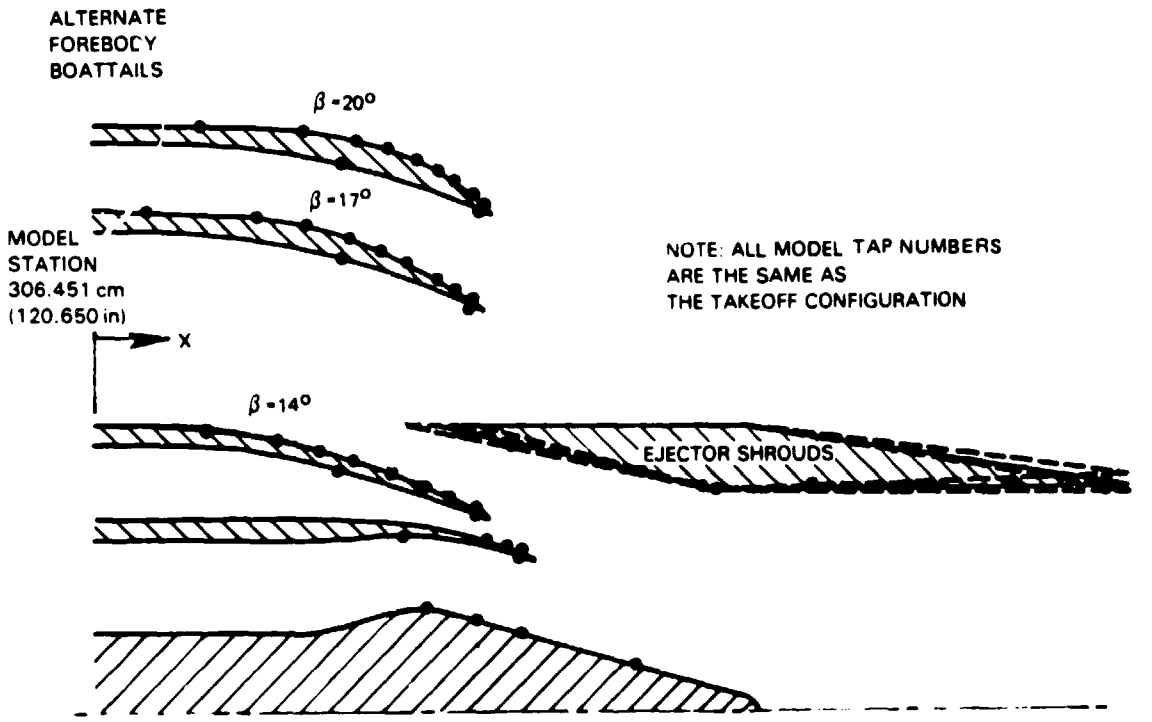

(b) Subsonic Cruise Configuration

Figure 3.2.5 Static Tap Locations

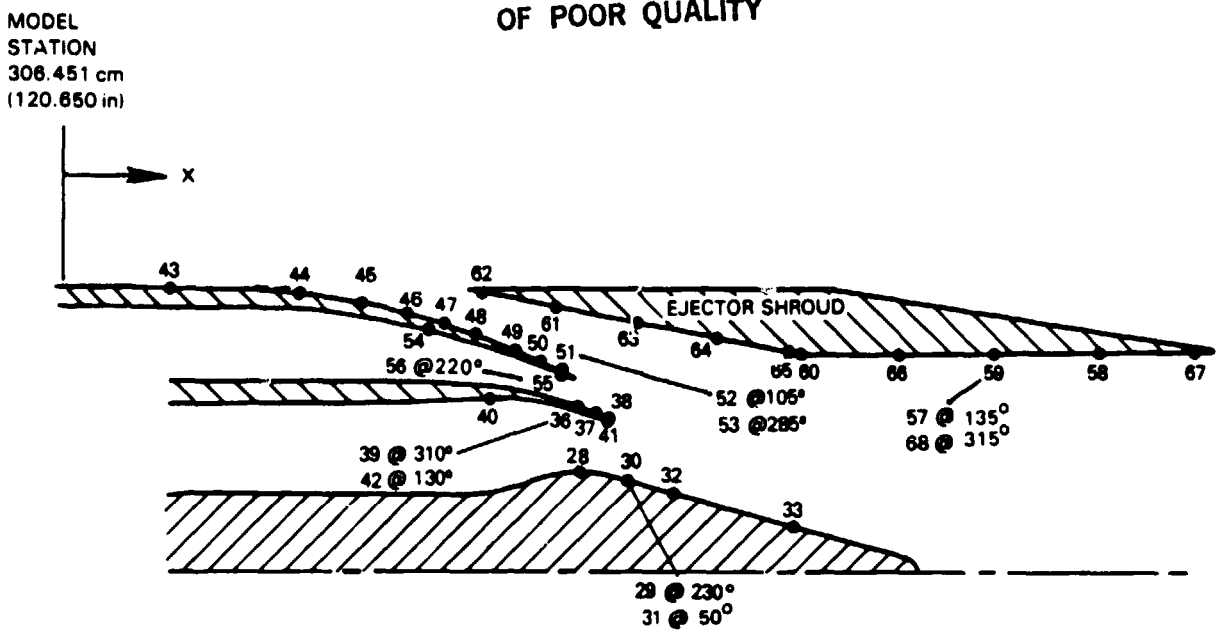

(c) Transonic Cruise Configuration - Ejector Inlet Open

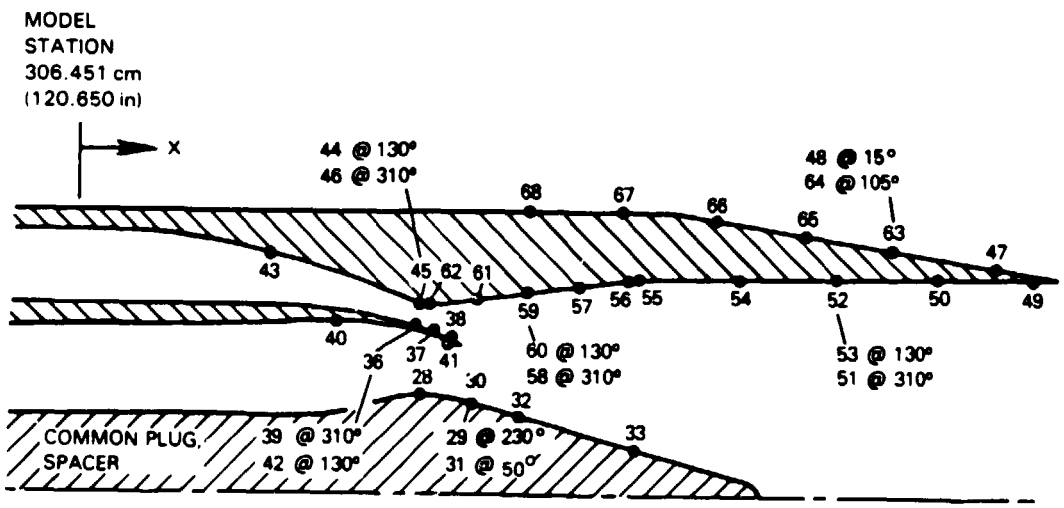

(d) Transonic Cruise Configuration - Ejector Inlet Closed

Figure 3.2-5 Static Tap Locations (Continued)

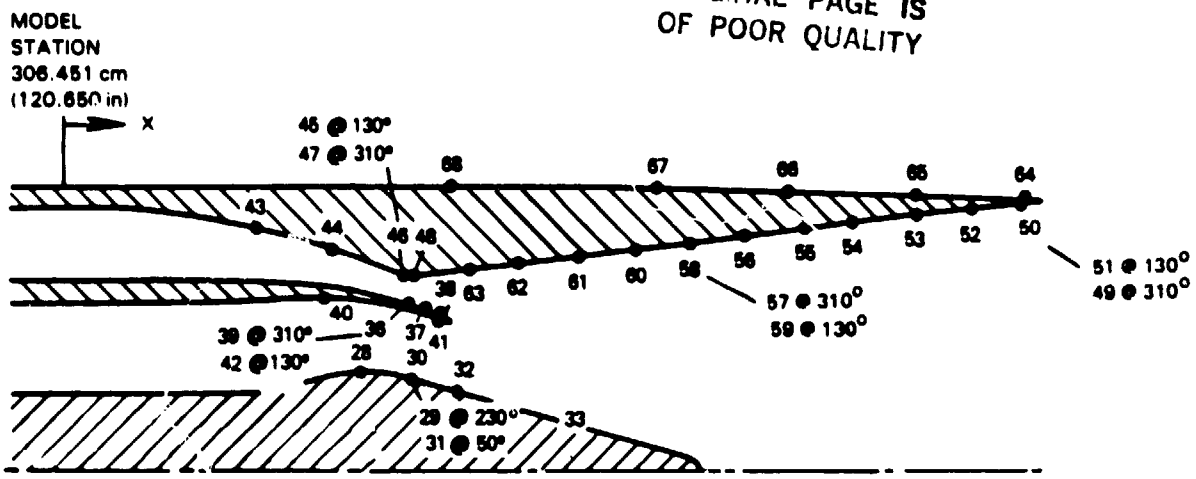

(e) Supersonic Cruise Configuration

Figure 3.2-5 Static Tap Locations (Concluded)

TABLE 3.2-III

Static Pressure Tap Locations
(Takeoff Configuration)

Plug

Tap Number	ϕ	X/D_{max}
28	320°	1.0007
29	320°	1.043
30	320°	1.043
31	50°	1.043
32	320°	1.123
33	320°	1.340

Flow Splitter

Tap Number	ϕ	X/D_{max}
36	40°	0.994
37	40°	1.027
38	40°	1.060
39	310°	0.994
40	320°	0.853
41	320°	1.060
42	130°	0.994

Forebody Boattail

Tap Number	ϕ	X/D_{max}
43	195°	0.265
44	195°	0.481
45	195°	0.594
46	195°	0.693
47	195°	0.771
48	195°	0.835
49	195°	0.890
50	195°	0.940
51	195°	0.990
52	105°	0.990
53	285°	0.990
54	40°	0.735
55	40°	0.990
56	220°	0.990

Ejector Shroud - Nominal Design
(Leading Edge at Station 326.258 cm
(128.448 in.)

Tap Number	ϕ	X/D_{max}
57	135°	1.774
58	225°	1.956
59	225°	1.774
60	225°	1.409
61	225°	1.053
62	225°	0.938
63	225°	1.169
64	225°	1.284
65	225°	1.399
66	225°	1.591
67	225°	2.138
68	315°	1.774

TABLE 3.2-III (Cont'd)

Static Pressure Tap Locations
(Subsonic Cruise Configuration)

Plug

Tap Number	ϕ	X/D_{max}
28	320°	0.953
29	320°	0.989
30	320°	0.989
31	50°	0.989
32	320°	1.069
33	320°	1.286

Flow Splitter

Tap Number	ϕ	X/D_{max}
36	40°	0.994
37	40°	1.027
38	40°	1.060
39	310°	0.994
40	320°	0.853
41	320°	1.060
42	130°	0.994

Forebody Boattail (β = 14°)

Tap Number	ϕ	X/D_{max}
43	195°	0.265
44	195°	0.492
45	195°	0.614
46	195°	0.698
47	195°	0.768
48	195°	0.829
49	195°	0.884
50	195°	0.935
51	195°	0.984
52	105°	0.984
53	285°	0.984
54	40°	0.735
55	40°	0.984
56	220°	0.984

Ejector Shroud - Nominal Design
(Leading Edge at Station 326.258 cm (128.448 in.)

Tap Number	ϕ	X/D_{max}
57	135°	1.774
58	225°	1.956
59	225°	1.774
60	225°	1.409
61	225°	1.053
62	225°	0.938
63	225°	1.169
64	225°	1.284
65	225°	1.399
66	225°	1.591
67	225°	2.138
68	315°	1.774

TABLE 3.2-III (Cont'd)

(Subsonic Cruise Configuration--Cont'd)

Forebody Boattail (β = 17°)

Tap Number	ϕ	X/D_{max}
43	195°	0.391
44	195°	0.586
45	195°	0.684
46	195°	0.752
47	195°	0.809
48	195°	0.859
49	195°	0.904
50	195°	0.947
51	195°	0.988
52	105°	0.988
53	285°	0.988
54	40°	0.735
55	40°	0.988
56	220°	0.988

Ejector Shroud - Nominal Design (Leading Edge at Station 326.730 cm (128.634 in.)

Tap Number	ϕ	X/D_{max}
57	135°	1.774
58	225°	1.956
59	225°	1.774
60	225°	1.409
61	225°	1.070
62	225°	1.960
63	225°	1.180
64	225°	1.289
65	225°	1.399
66	225°	1.591
67	225°	2.138
68	315°	1.774

Forebody Boattail (β = 20°)

Tap Number	ϕ	X/D_{max}
43	195°	0.480
44	195°	0.668
45	195°	0.759
46	195°	0.820
47	195°	0.868
48	195°	0.909
49	195°	0.942
50	195°	0.972
51	195°	0.997
52	105°	0.997
53	285°	0.997
54	40°	0.735
55	40°	0.997
56	220°	0.997

Ejector Shroud - Nominal Design (Leading Edge at Station 327.607 cm (128.979 in.)

Tap Number	ϕ	X/D_{max}
57	135°	1.774
58	225°	1.956
59	225°	1.774
60	225°	1.409
61	225°	1.099
62	225°	0.999
63	225°	1.199
64	225°	1.299
65	225°	1.399
66	225°	1.591
67	225°	2.138
68	315°	1.774

TABLE 3.2-III (Cont'd)

Static Pressure Tap Locations
(Transonic Cruise Configuration)

Plug

Tap Number	ϕ	X/D_{max}
28	320°	1.091
29	230°	1.127
30	320°	1.127
31	50°	1.127
32	320°	1.207
33	320°	1.424

Flow Splitter

Tap Number	ϕ	X/D_{max}
36	40°	0.994
37	40°	1.027
38	40°	1.060
39	310°	0.994
40	320°	0.853
41	320°	1.060
42	130°	0.994

Forebody Boattail

Tap Number	ϕ	X/D_{max}
43	195°	0.265
44	195°	0.490
45	195°	0.610
46	195°	0.705
47	195°	0.777
48	195°	0.836
49	195°	0.888
50	195°	0.938
51	195°	0.986
52	105°	0.986
53	285°	0.986
54	40°	0.735
55	40°	0.986
56	220°	0.986

Ejector Shroud - Nominal Design
(Leading Edge at Station 323.908 cm
(127.523 in.)

Tap Number	ϕ	X/D_{max}
57	135°	1.774
58	225°	1.956
59	225°	1.774
60	225°	1.409
61	225°	1.053
62	225°	0.938
63	225°	1.169
64	225°	1.284
65	225°	1.399
66	225°	1.591
67	225°	2.138
68	315°	1.774

TABLE 3.2-III (Cont'd)

(Transonic Cruise Configuration--Cont'd)

Ejector Inlet Closed Shroud

Tap Number	ϕ	X/D_{max}	Tap Number	ϕ	X/D_{max}
43	40°	0.735	56	40°	1.399
44	130°	1.006	57	40°	1.303
45	40°	1.006	58	310°	1.208
46	310°	1.006	59	40°	1.208
47	195°	2.069	60	130°	1.208
48	15°	1.884	61	40°	1.112
49	40°	2.138	62	40°	1.016
50	40°	1.956	63	195°	1.884
51	310°	1.774	64	105°	1.884
52	40°	1.774	65	195°	1.712
53	130°	1.774	66	195°	1.548
54	40°	1.591	67	195°	1.382
55	40°	1.409	68	195°	1.206

TABLE 3.2-III (Concluded)

Static Pressure Tap Locations
(Supersonic Cruise Configuration)

Plug			Flow Splitter		
Tap Number	ϕ	X/D_{max}	Tap Number	ϕ	X/D_{max}
28	320°	1.007	36	40°	0.994
29	230°	1.043	37	40°	1.027
30	320°	1.043	38	40°	1.060
31	50°	1.043	39	310°	0.994
32	320°	1.123	40	320°	0.853
33	320°	1.340	41	320°	1.060
			42	130°	0.994

Shroud					
Tap Number	ϕ	X/D_{max}	Tap Number	ϕ	X/D_{max}
43	40°	0.735	56	40°	1.631
44	40°	0.874	57	310°	1.528
45	130°	1.008	58	40°	1.528
46	40°	1.008	59	130°	1.528
47	310°	1.008	60	40°	1.426
48	40°	1.018	61	40°	1.324
49	310°	2.141	62	40°	1.222
50	40°	2.141	63	40°	1.120
51	130°	2.141	64	195°	2.141
52	40°	2.039	65	195°	1.936
53	40°	1.937	66	195°	1.703
54	40°	1.835	67	195°	1.470
55	40°	1.733	68	195°	1.088

3.2.3 Test Matrix

A test matrix showing the combinations of geometric and aerodynamic variables tested is provided in Table 3.2-IV. The ejector inlet and exit areas described are normalized by the sum of the fan and primary nozzle jet area (a_j) established for each flight condition. For each configuration tested, fan nozzle pressure ratic (P_{tf}/P_0) was varied over the described range at fixed values of fan-to-primary total pressure split (P_{tf}/P_{tp}). The range of nozzle pressure ration and total pressure split for each flight condition is nominal variations about the engine operating point described in Section 3.2.

TABLE 3.2-IV

Test Matrix

TEST CONDITION	FAN NOZZLE PRESSURE RATIO Ptf/Po	FAN-TO-PRIMARY TOTAL PRESSURE SPLIT Ptf/Ptp	FOREBODY BOATTAIL ANGLE β DEGREES	EJECTOR INLET AREA FAN+PRIM NOZZLE AREA Ain/Aj	EJECTOR EXIT AREA FAN+PRIM NOZZLE AREA Aex/Aj	FAN DUCT NOZZLE AREA Ajf cm^2 (in^2)	PRIMARY NOZZLE AREA Ajp cm^2 (in^2)
TAKEOFF Mo=0, 0.36	2.0-3.8	1.6, 1.78, 1.9	11.7	0.67,0.73,0.87	1.60,1.71,1.88	61.258(9.495)	68.193(10.570)
SUBSONIC CRUISE Mo=0.9	3.8-6.2	1.8,2.05,2.2	14 17 20	0.82,1.0,1.19,0* 0.72,1.0,1.14 0.98	1.90,2.04,2.24,0* 1.90,2.04,2.24 2.04	34.129(5.290)	74.516(11.550)
TRANSONIC CRUISE Mo=1.2	5.8-8.8	1.1,1.35,1.6	13.5	0.63,0.75 CLOSED	2.28 2.28	38.961(6.039)	58.265(9.031)
SUPERSONIC CRUISE Mo=2.0	20-30	1.8,2.12,2.4	--	CLOSED	2.95	44.122(6.839)	68.193(10.570)

*Ejector Removed

SECTION 4.0

DATA REDUCTION PROCEDURES

General descriptions of the equations used to define model flow rates, nozzle thrust, and boattail drag are contained in this section. All constants and equations are presented as actually used during the data reduction process.

4.1 FAN AND PRIMARY FLOW RATES

Both fan and primary mass flow rates were measured with choked venturi. These flow rates were calculated using the measured air total temperature, T_{tv}, and pressure, P_{tv}, respectively, and eq. (1).

$$m_v = C_{dv} \frac{K_v Pt_v A_v}{\sqrt{Tt_v}} \tag{1}$$

where C_{dv} is the venturi discharge coefficient, K_v is the critical flow factor, and A_v is the geometric throat area of the venturi.

The venturi discharge coefficient was based on analytical techniques for choked venturis with circular arc throats. This coefficient accounts for viscous effects and sonic line distortion at the venturi throat. The critical flow factor, K_v, is a function of total pressure and temperature and accounts for real gas effects. The critical flow factor was obtained by curve-fitting tabulated values from reference 10.

Total pressure, P_{tv}, was determined by measuring the static pressure, P_v, upstream of the venturi throat and calculating the total pressure as

$$Pt_v = P_v/C \tag{2}$$

The factor C, a constant for a given venturi, is the one-dimensional static-to-total-pressure ratio corresponding to the ratio of the area at the measuring plane to area of the venturi throat. The static pressure was measured by four taps. Venturi total temperature, T_{tv}, was determined using three iron-constantan thermocouples located upstream of each venturi; the three readings were averaged.

4.2 FLOW COEFFICIENTS

The flow coefficient of a nozzle is the ratio of actual mass flow through the nozzle to the ideal isentropic flow rate at the temperature and pressure of the flow (eq. 3).

$$C_d = \frac{m}{m_i} \tag{3}$$

Ideal flow rate is calculated from the following equation

$$m_i = \frac{KP_tA}{\sqrt{T_t}} \left(\frac{A^*}{A}\right) \tag{4}$$

where A, P_t, and T_t are the nozzle geometric throat area, total pressure, and total temperature, respectively

The critical flow factor, K, a function of nozzle total pressure and temperature, is obtained by curve-fitting tabulated values from reference 10. Area ratio A*/A is the ratio of flow area at sonic conditions to the nozzle throat area. For values of nozzle pressure ratio, P_t/P_0, greater than 1.8929, A*/A in the ideal weight flow equation is equal to one. For lower pressure ratios, A*/A is calculated from one-dimensional, isentropic relationships

$$A8/A = \frac{216}{125} M \left(1 + \frac{M^2}{5}\right)^{-3} \tag{5}$$

where

$$M = \left\{ 5 \left[\left(P_t/P_0\right)^{0.28571} - 1 \right] \right\}^{1/2} \tag{6}$$

4.3 THRUST MEASUREMENTS

The nozzle-generated thrust-minus-drag for this test was defined as the axial exit momentum of the exhaust flow plus the excess of exit pressure over ambient pressure times the exit area normal to the axis, minus the axial pressure drag on the nozzle external surfaces (i.e., trailing edge flaps and forebody inlet boattails).

$$F - D_{ex} = \int_{A_{exit}} d(mV)_{axial} + \int_{A_{exit}} (P_{exit} - P_0)dA - D_{ex} \tag{7}$$

Thus, this definition of thrust-minus-drag does not penalize the nozzle for external friction drag. This definition of thrust is consistent with the bookkeeping for calculating airframe-installed nozzle performance in which the nozzle external friction drag is accounted for at the correct Reynolds number for a specific flight condition.

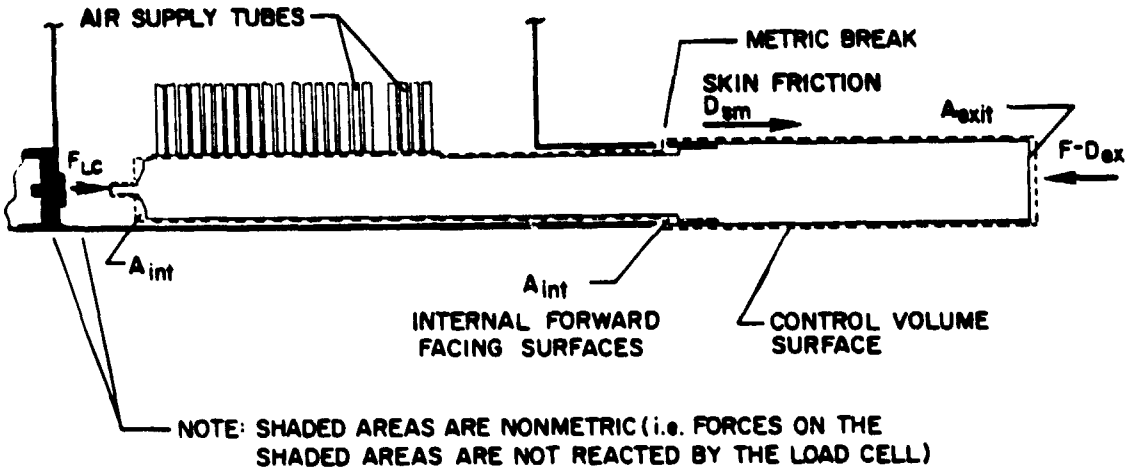

Figure 4.3-1 Control Volume for 21.59 cm (8.5 in.) Model Thrust Determination

Figure 4.3-1 above shows the control volume applied to the test nozzles. The momentum equation in the axial direction for this control volume demonstrates how thrust was measured for this test

$$F_{LC} + \sum P_{int} A_{int} - P_{exit}A_{exit} + D_{sm} + D_{ex} = mV_{exit} \qquad (8)$$

Substituting eq. (7) for mV_{exit} in eq. (8) then

$$F_{LC} + \sum P_{int}A_{int} - P_{exit}A_{exit} + D_{sm} + D_{ex} = (F - D_{ex}) - (P_{exit} - P_o)A_{exit} + D_{ex} \qquad (9)$$

rearranging and cancelling terms

$$F - D_{ex} = F_{LC} + P_{int}A_{int} - P_oA_{ext} + D_{sm} \qquad (10)$$

But

$$P_oA_{exit} = P_o\sum A_{int} \qquad (11)$$

Therefore

$$F - D_{ex} = F_{LC} + \sum A_{int}(P_{int} - P_o) + D_{sm} \tag{12}$$

F_{LC} is the axial force measured by the load cell, calibrated by applying a known force and correlating this force against the load cell output. Thus, this calibration provided a linear relationship between the applied load and the load cell output in millivolts, used to determine the load cell force

$$F_{LC} = a(mv) + b \tag{13}$$

where a and b are constants determined by the calibrations, and m_v is the load cell reading in millivolts.

The term A_{int} $(P_{int} - P_o)$ accounts for internal pressure shear forces acting on the forward facing surfaces (A_{int}) of the metric part of the model. The internal pressure, P_{int}, was measured with two static pressure taps 180 degrees apart at each of the forward facing surfaces. As indicated by eq. (12), an adjustment was made to the measured thrust-minus-drag of the nozzles to account for external skin friction drag (D_{sm}) acting on the cylindrical section of the model downstream of the metric break. External skin friction drag was estimated using the method reported in reference 11.

4.4 THRUST COEFFICIENTS

The nozzle thrust coefficient is defined as the ratio of measured nozzle gross thrust-minus-drag to the sum of the ideal thrusts of the fan and primary streams. As noted, the thrust-minus-drag for this data reduction procedure does not penalize the nozzle for external skin friction drag. Ideal thrust for each stream equals the mass flow rate times the ideal velocity, i.e., the velocity of the stream expanded isentropically from the upstream total pressure to the ambient pressure. The equation for the thrust coefficient is thus

$$C_f = \frac{F - D_{ex}}{m_f V_{if} + m_p V_{ip}} \tag{14}$$

The ideal thrust for each stream was calculated using the dimensionless ideal thrust function, which is a function of nozzle pressure ratio (P_t/P_o) and the ratio of specific heats γ.

$$\frac{m_i V_i}{P_t A^*} = \gamma \left(\frac{2}{\gamma + 1}\right)^{\frac{\gamma}{\gamma - 1}} \left(\frac{\gamma + 1}{\gamma - 1}\right)^{1/2} \left[1 - (p_o/P_t)^{\frac{\gamma - 1}{\gamma}}\right]^{1/2} \tag{15}$$

or

$$\frac{m_i V_i}{P_t A^*} = 1.81163 \sqrt{1 - (P_o/P_t)^{0.28571}} \quad \text{for } Y = 1.4 \tag{16}$$

The ideal thrust for the fan and primary streams is then

$$m_f V_{if} = C_{df} Pt_f A_f \left(\frac{A^*}{A}\right)_f \left(\frac{m_i V_i}{P_t A^*}\right)_f \tag{17}$$

$$m_p V_{ip} = C_{dp} Pt_p A_p \left(\frac{A^*}{A}\right)_p \left(\frac{m_i V_i}{P_t A^*}\right)_p \tag{18}$$

For pressure ratios greater than 1.8929, A*/A = 1.0. For pressure ratios less than this, A*/A is calculated as described in Section 4.2 on flow coefficients.

4.5 FOREBODY BOATTAIL PRESSURE DRAG

Pressure drag on the forebody boattail surface was calculated for the takeoff, subsonic cruise, and transonic cruise ejector configurations where the ejector inlet is opened. The boattail pressure drag, D_β, is simply defined as the integrated difference between the surface static pressure and ambient pressure on the boattail projected frontal area, as follows

$$D_\beta = -\int_A (P - Po)\, dA \tag{19}$$

A pressure coefficient, C_p, may be defined as the difference between the measured surface static pressure and ambient pressure divided by the freestream dynamic pressure

$$C_p = (P - Po)/q_o \tag{20}$$

In addition, a boattail pressure drag coefficient, $C_{D\beta}$, may be defined as the boattail pressure drag divided by the freestream dynamic pressure and a reference cross-sectional area

$$C_{D\beta} = D\beta / q_o A_{Ref} \tag{21}$$

After substitution of terms, the expression for pressure drag coefficient becomes

$$C_{D\beta} = -\int_A (C_p\, dA)/A_{Ref} \tag{22}$$

For the test program, pressure coefficients were calculated for each boattail pressure tap. Representative segments of boattail projected frontal area, A, were assigned to each pressure tap. The model maximum cross-sectional area, 366.096 cm^2 (56.745 $in.^2$), was selected as the reference area. The boattail pressure drag coefficient then becomes a summation

$$C_{D\beta} = - \frac{\sum(C_p \Delta A)}{56.745} \tag{23}$$

The loss in thrust coefficient, ΔC_F, is the boattail pressure drag divided by the nozzle ideal thrust

$$\Delta C_F = \frac{\sum(P - Po)\,\Delta A}{m_f V_{if} + m_p V_{ip}} \tag{24}$$

The ideal thrust terms were obtained from eq. (17) and (18).

Table 4.5-I lists the nominal representative segments of boattail projected frontal area, ΔA, assigned to each boattail pressure tap in the data reduction calculations.

Table 4.5-I

Assigned Forebody Boattail Projected Areas

Model Tap No.	Configuration: Takeoff cm^2	Takeoff $in.^2$	Subsonic Cruise cm^2	Subsonic Cruise $in.^2$	Transonic Cruise cm^2	Transonic Cruise $in.^2$
43	0	0	0	0	0	0
44	22.548	3.495	25.843	4.0056	25.284	3.919
45	22.548	3.495	25.843	4.0056	25.284	3.919
46	22.548	3.495	25.843	4.0056	25.284	3.919
47	22.548	3.495	25.843	4.0056	25.284	3.919
48	22.548	3.495	25.843	4.0056	25.284	3.919
49	22.548	3.495	25.843	4.0056	25.284	3.919
50	22.548	3.495	25.843	4.0056	25.284	3.919
51	7.516	1.165	8.614	1.3352	8.428	1.3064
52	7.516	1.165	8.614	1.3352	8.428	1.3064
53	7.516	1.165	8.614	1.3352	8.428	1.3064

SECTION 5.0

RESULTS AND DISCUSSION

5.1 NOZZLE THRUST PERFORMANCE

A discussion of the nozzle thrust performance and flow characteristics of the configurations tested is presented in this section and includes the effects of the geometric and aerodynamic variables evaluated at each simulated flight condition. Also, the measured thrust performance is compared to the previous ejector nozzle test results and to the performance goals assumed for the Advanced Supersonic Transport propulsion studies. Emphasis is placed on the analysis of the nozzle performance obtained at the simulated engine operating conditions.

The discussion is organized to present the performance characteristics first, in the order of ascending flight Mach number from takeoff to supersonic cruise. Performance comparisons are then addressed and the discussion is concluded with a presentation of the nozzle flow coefficients.

5.1.1 Takeoff Performance at Mach Number of 0 and 0.36

A comparison of nozzle thrust performance C_f, at quiescent, and M_o = 0.36 flyover conditions is presented in Figure 5.1-1 for the range of fan nozzle pressure ratio, P_{tf}/P_o, and fan-to-primary pressure split, P_{tf}/P_{tp}, tested. The collapse of each data set (M_o = 0 and 0.36) as a function of fan-to-primary pressure split shows that takeoff configuration performance is not influenced by the range of P_{tf}/P_{tp} tested. At the nominal nozzle operating conditions, P_{tf}/P_o of 2.84 and P_{tf}/P_{tp} of 1.78, the comparison shows that the freestream flow effects at M_o = 0.36 reduced the level of quiescent performance, C_f = 0.983, by 1.3 percent. The loss of performance with external flow is attributed to the ejector shroud and inlet forebody boattail drags and the induced drag of the ejector inlet flow. The impact of external flow on static performance was also found to be a function of ejector inlet and exit area, Ain/Aj and Aex/Aj, as described in the following paragraph.

To determine the influence of ejector inlet and exit area on takeoff performance, nine configurations were tested over a range of areas at quiescent and fly-over conditions. Results of these tests were correlated to provide performance maps with lines of constant C_f plotted as a function of normalized ejector exit and inlet areas, A_{ex}/A_j and A_{in}/A_j, at the nominal takeoff operating conditions, as shown in Figure 5.1-2a and b. The static performance map, Figure 5.1-2a, shows that performance increases with decreasing exit area and increasing inlet area to a maximum value of 0.983 at an A_{ex}/A_j of 1.60 and A_{in}/A_j of 0.87. The trend of increasing C_f with decreasing exit area is due to a reduction of the fan and primary jet overexpansion losses with decreasing exit area as the ejector configuration tends to operate like a convergent-divergent (C-D) nozzle. The quantity of ejector inlet flow required to minimize overexpansion losses is also reduced with decreasing exit area.

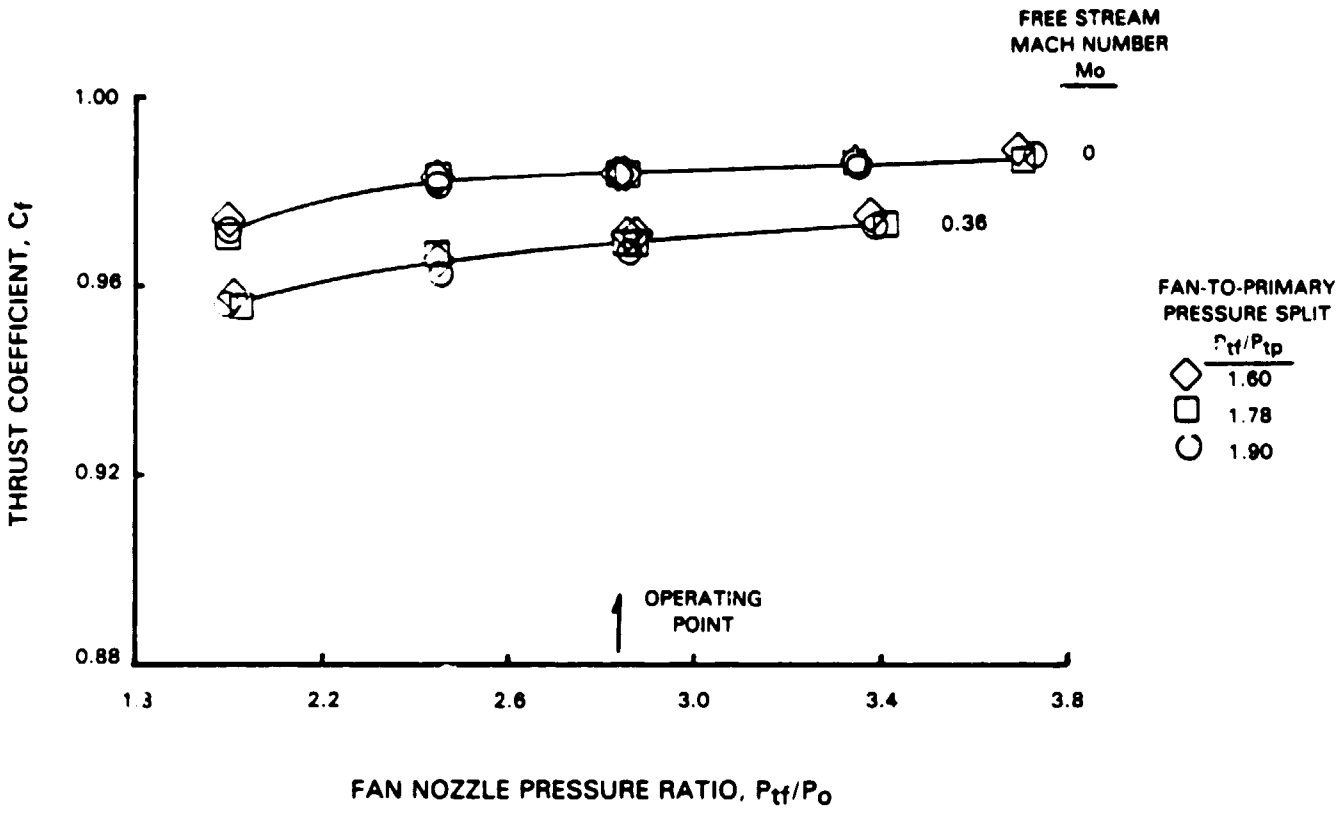

Figure 5.1-1 Comparison of Takeoff Performance at Quiescent and M_o = 0.36 Freestream Conditions for Various Fan-to-Primary Pressure Splits Tested. Ejector Inlet and Exit Area Ratio: A_{in}/A_j, 0.87; A_{ex}/A_j, 1.71.

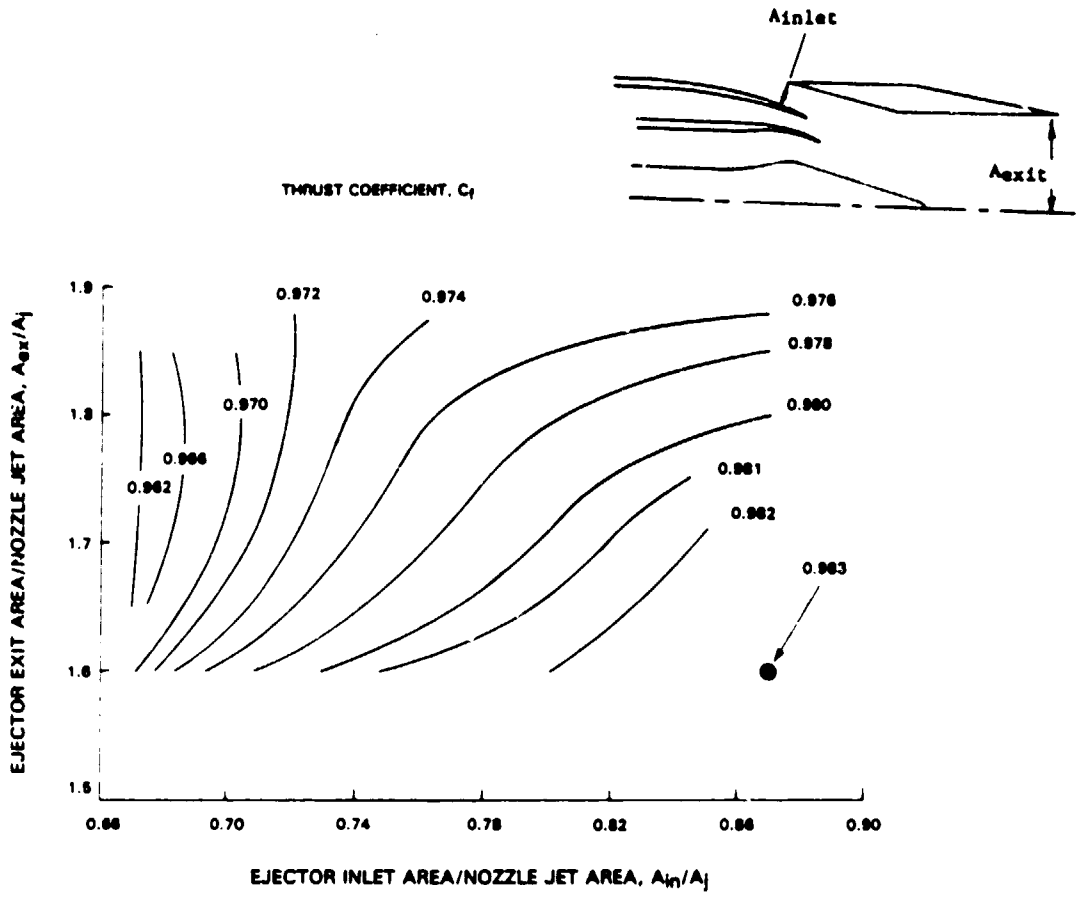

(a) Freestream Mach Number, M_n, 0.

Figure 5.1-2 Takeoff Configuration Ejector Performance Maps. Conditions: Fan-to-Primary Pressure Split, P_{tf}/P_{tp}, 1.78; Fan Nozzle Pressure Ratio, P_{tf}/P_0, 2.84.

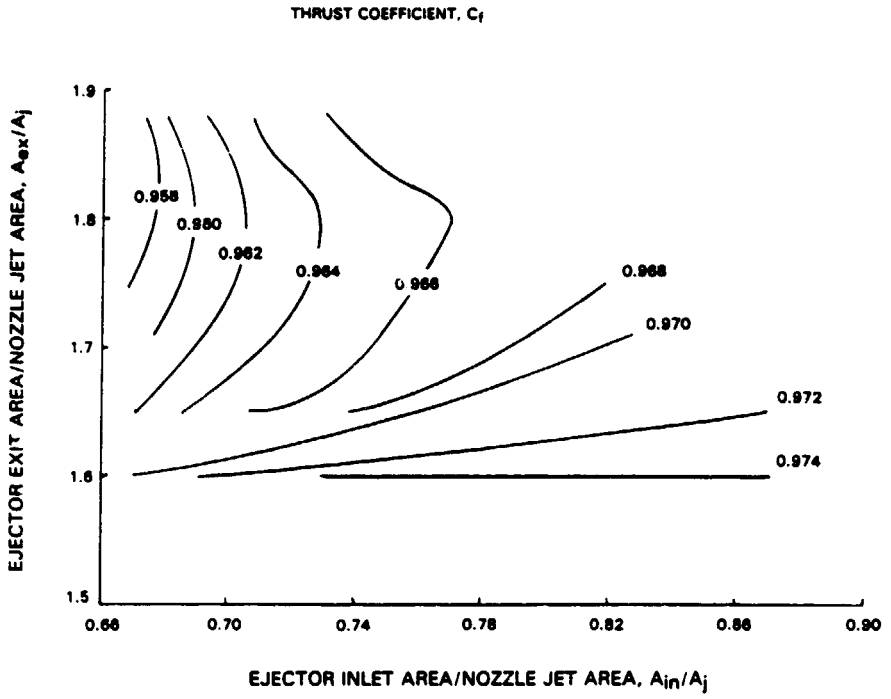

(b) Freestream Mach Number, M_0, 0.36.

Figure 5.1-2 Takeoff Configuration Ejector Performance Maps. Conditions: Fan-to-Primary Pressure Split, P_{tf}/P_{tp}, 1.78; Fan Nozzle Pressure Ratio, P_{tf}/P_0, 2.84. (Concluded)

The trend of increasing performance with increasing inlet area is a result of two mechanisms: 1) increasing inlet area increases secondary flow to reduce overexpansion losses and 2) at static conditions, the thrust augmentation of the secondary flow increases with increasing inlet area. The performance map for the M_0 0.36 fly-over conditions, Figure 5.1-2b, also shows similar trends of increasing C_f with decreasing exit area and increasing inlet area. However, it is observed that maximum performance, C_f = 0.974, is 0.9 percent lower than the peak static results. The loss in performance relative to the static results is due to the freestream flow drag effects discussed in the previous paragraph. It is also observed that the maximum performance occurred over a range of moderate to large inlet area, A_{in}/A_j of 0.73 to 0.87, whereas the peak static performance occurred only at the largest inlet area tested. This difference in performance characteristic as a function of inlet area is due to the induced inlet flow drag (ram plus spillage drag) associated with the freestream flow. The induced drag increasing with increasing inlet flow area cancels any increase in secondary flow thrust augmentation.

5.1.2 Subsonic Cruise Performance at 0.9 Mach Number

The influence of fan-to-primary pressure split, P_{tf}/P_{tp}, on subsonic cruise performance is shown in Figure 5.1-3 as a function of fan nozzle pressure ratio, P_{tf}/P_0. These data were acquired for the 14° forebody boattail configuration with the ejector inlet and exit areas set at Ain/Aj = 0.82 and Aex/Aj = 1.90. A comparison of the three data sets shows that P_{tf}/P_{tp} does influence subsonic cruise performance, the performance tending to increase with decreasing pressure split.

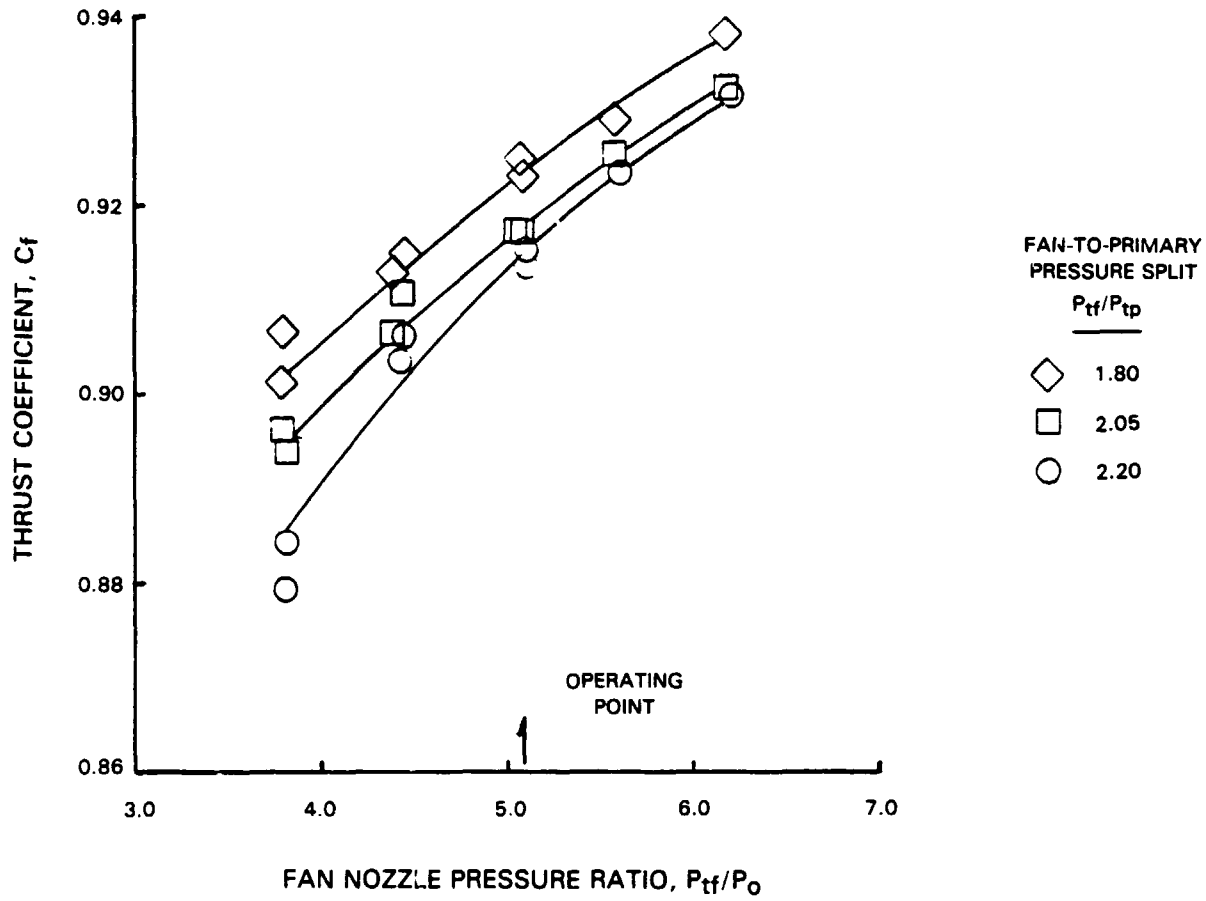

Figure 5.1-3 Influence of Fan-to-Primary Pressure Split on Subsonic Cruise Performance, Freestream Mach Number, M_0, 0.9. Configuration: Forebody Boattail Angle, β , 14°; Ejector Inlet and Exit Area Ratio, A_{in}/A_j, 0.82; A_{ex}/A_j, 1.90

These results indicate that highest nozzle performanance, C_f = 0.923, is obtained at a 1.80 pressure split, whereas the VSCE engine is scheduled to operate at a P_{tf}/P_{tp} of 2.05. The engine could be operated at a lower pressure split by rescheduling the variable geometry, but the installed performance would be adversely affected by increased engine inlet spillage

drag and increased fuel consumption due to the change in engine cycle. Unfortunately it was not possible to conduct the installed performance trade studies required to evaluate the net effect of these changes. The higher performance associated with decreasing pressure split is a result of two factors: 1) the increase in primary flow with decreasing P_{tf}/P_{tp} tends to reduce the overexpansion losses and 2) at a constant fan nozzle pressure ratio the increasing primary flow results in an increasing nozzle thrust while the drag associated with the M_0 0.9 freestream flow remains relatively constant. The trend of rapidly increasing performance with increasing fan nozzle pressure ratio indicates that nozzle flow is greatly overexpanded at the lower pressure ratios, noting that A_{ex}/A_j for this configuration is 1.90.

Tests were conducted with the 14° forebody boattail/ejector configurations to determine the influence of ejector inlet and exit area on subsonic cruise performance. These data are presented as an ejector inlet and exit area performance map in Figure 5.1-4 at the nominal nozzle operating conditions. For these conditions (P_{tf}/P_0 = 5.09 and P_{tf}/P_{tp} = 2.05) performance increased with both decreasing exit and inlet area to a maximum value of C_f = 0.917 at the minimum areas tested, A_{in}/A_j = 0.82 and A_{ex}/A_j = 1.90. Further reductions in inlet or exit area may yield higher nozzle performance. The trend of increasing performance with decreasing exit area is again explained by a reduction in overexpansion losses and also a reduction of ejector inlet flow required to minimize overexpansion. The trend of increasing performance with decreasing inlet area (i.e., decreasing inlet flow) is a result of a trade off between the inlet flow required to minimize overexpansion thrust loss and the drag penalty of the inlet flow, as illustrated in Figure 5.1-5.

The effect of the ejector on the subsonic cruise performance of the basic 14° boattail coannular nozzle was determined by testing the configuration with the ejector removed. A comparison of the coannular nozzle performance with the ejector removed to the best performing ejector configuration, A_{in}/A_j = 0.82 and A_{ex}/A_j = 1.90, is presented in Figure 5.1-6. The comparison shows that with the ejector removed the performance of the coannular nozzle with the 14° forebody boattail increased 1.4 percent (C_f = 0.931) at the nominal operating conditions. An analysis of the ejector drag penalty, ΔC_f = 0.014, was conducted to determine the breakdown of the total loss in terms of ejector shroud form (pressure) drag and internal friction drag, recalling that the external friction drag has been removed from the data as acquired. It is estimated that of the total 0.014 ΔC_f drag penalty the internal shroud friction drag increment is 0.005 ΔC_f and the remaining loss increment, 0.009 ΔC_f, is attributed to shroud inlet and form drag.

Experience in the development of the F-111 ejector nozzle has shown that through development and refinement of the shroud geometry, the inlet and form drag portion of the ejector drag penalty can be eliminated or minimized depending on other shroud design constraints such as tail-feather hinge location, actuation hardware, reverser requirements, and other structural considerations. As the tested ejector design is preliminary in nature, it could be expected that through development the estimated shroud drag penalty,

ΔC_f of 0.009, could be reduced or eliminated. If these refinements were pursued the performance potential of the 14° boattail subsonic cruise configuration could be as high as a thrust coefficient of 0.926 for P_{tf}/P_0 = 5.09 and P_{tf}/P_{tp} = 2.05.

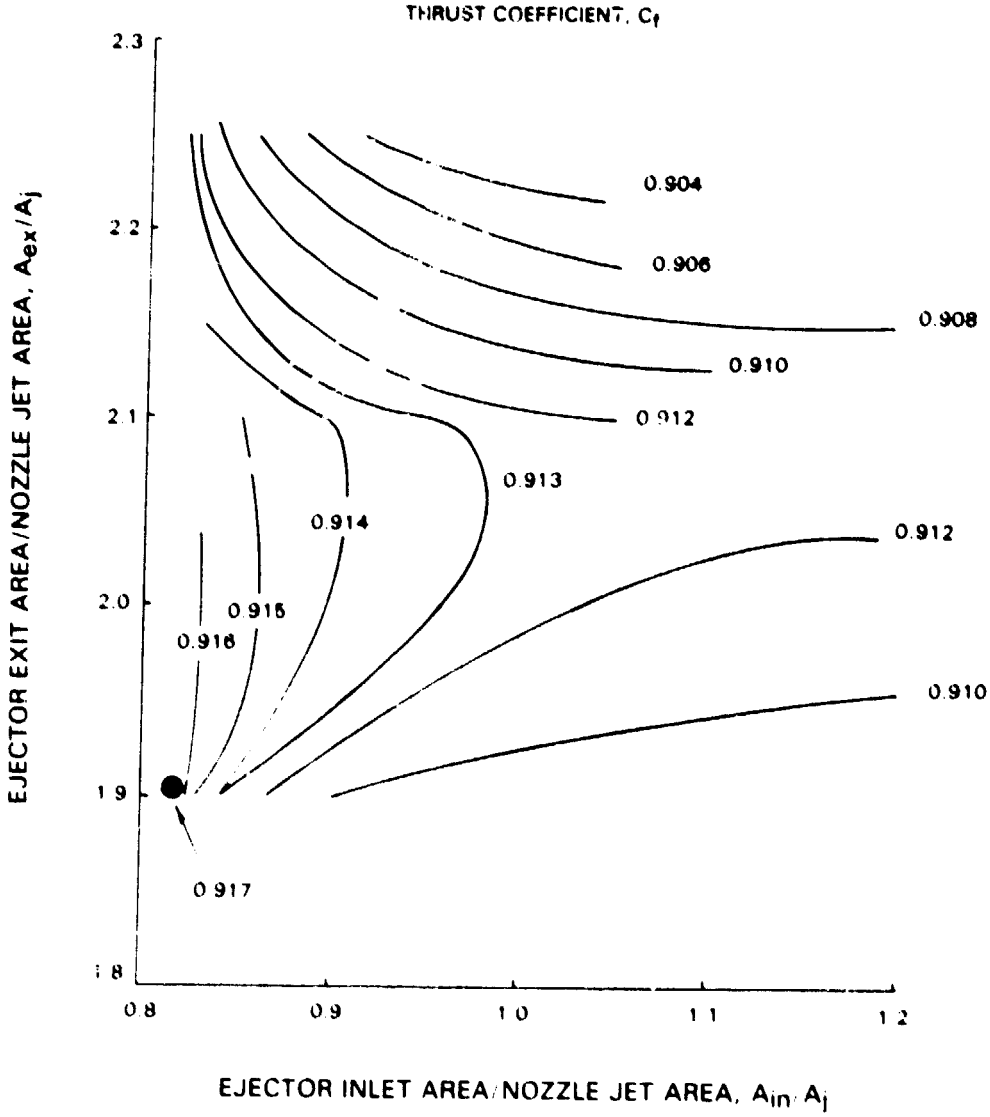

Figure 5.1-4 Subsonic Cruise Configuration Ejector Performance Map With Forebody Boattail Angle, β, 14°. Conditions: Freestream Mach Number, M_0, 0.9; Fan-to-Primary Pressure Split, P_{tf}/P_{tp}, 2.05; Fan Nozzle Pressure Ratio, P_{tf}/P_0, 5.09.

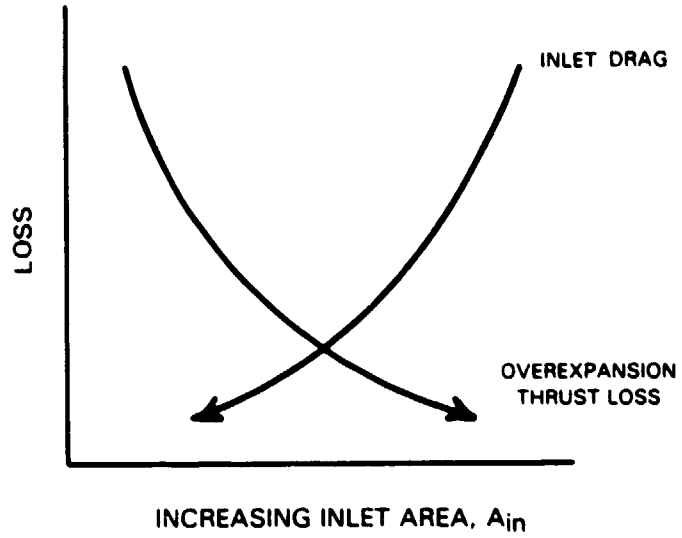

Figure 5.1-5 Trade-Off of Over Expansion Thrust Loss and Inlet Drag

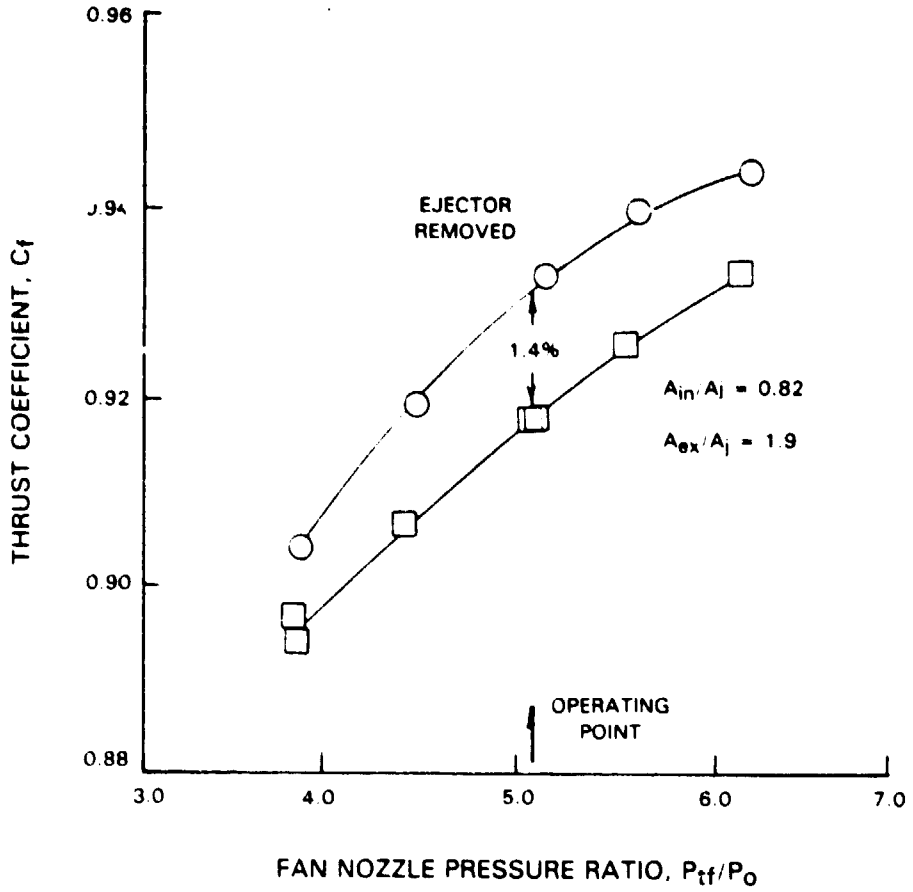

Figure 5.1-6 Effect of Ejector on Subsonic Cruise Performance with 14° Forebody Boattail. Conditions: Freestream Mach Number, M_o, 0.9; Fan-to-Primary Pressure Split, P_{tf}/P_{tp}, 2.05.

The previous discussion indicates that in the development of an ejector nozzle system, the level of performance of the basic nozzle configuration with the ejector removed, in this case a C_f of 0.931 at the engine operating point, may be approached but not exceeded because of the shroud friction drag. Therefore, further increases in ejector nozzle performance can only be achieved with a reduction in losses of the basic nozzle configuration. For the basic coannular nozzle tested with the ejector removed, these losses consist of internal nozzle thrust loss and boattail form drag associated with the 14° forebody boattail, again keeping in mind that the external friction drag has been removed from the data presented.

The 0.9 M_0 boattail drag increment was determined to be 0.054 ΔC_f by integrating the static pressure distribution measured over the boattail projected area as shown in Figure 5.1-7. The internal coannular nozzle performance was determined to be 0.985 by adding the boattail loss increment, $\Delta C_f = 0.054$, to the measured performance of the basic nozzle, $C_f = 0.931$. This level of performance is considered acceptable for a coannular nozzle. The bookkeeping procedure is shown graphically in Figure 5.1-8. Further improvements in subsonic cruise performance above a C_f of 0.926 at the engine operating point can only be realized by a reduction in forebody boattail loss as there is little room for improvement of the internal nozzle performance. The influence of boattail geometry on nozzle performance is addressed in the following discussion.

The effect of forebody boattail geometry on performance was evaluated by testing elliptical arc boattails of 14°, 17°, and 20° mean angles at the nominal design ejector setting, $A_{in}/A_j + 1.0$ and $A_{ex}/A_j = 2.04$. The results of these tests at the nominal nozzle operating conditions, Figure 5.1-9, show that performance decreases with increasing angle from a C_f of 0.912 at 14° to a C_f of 0.901 at 20°. Examination of the static pressure distributions over the boattails indicates the loss of performance with increasing angle is related to flow separation over the aft portion of the steeper boattails. The pressure distribution, C_p, over the three boattails are presented in Figure 5.1-10 as a function of normalized forebody boattail length, L/D_{max}. Analysis of the distributions over the 17° and 20° boattails shows that after the initial acceleration the pressure recovery over the aft portion of the two boattails is increasing but then levels off, indicating the onset of flow separation, whereas the pressure recovery over the 14° boattail continues to increase to the trailing edge, indicating attached flow. A detailed investigation of the 17° and 20° boattail distributions shows that the flow separation occurs over a greater portion of the 20° boattail than the 17° boattail which explains the lower performance of the 20° configuration. The trend of increasing performance with decreasing boattail angle, Figure 5.1-9, suggests that a further reduction in boattail angle would yield higher subsonic cruise performance, but at the expense of increased nozzle length and weight.

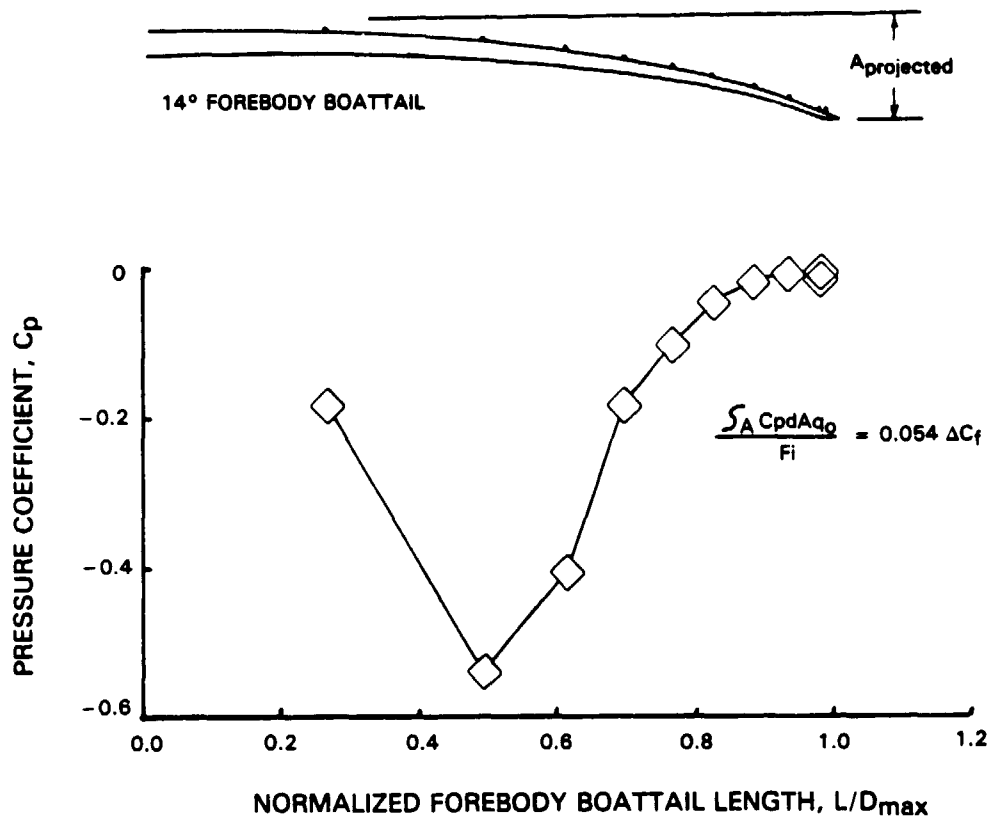

Figure 5.1-7 Static Pressure Distribution Over 14° Forebody Boattail With Ejector Removed. Conditions: Freestream Mach Number, M_o, 0.9; Fan-to-Primary Pressure Split, P_{tf}/P_{tp}, 2.05; Fan Nozzle Pressure Ratio, P_{tf}/P_o, 5.09.

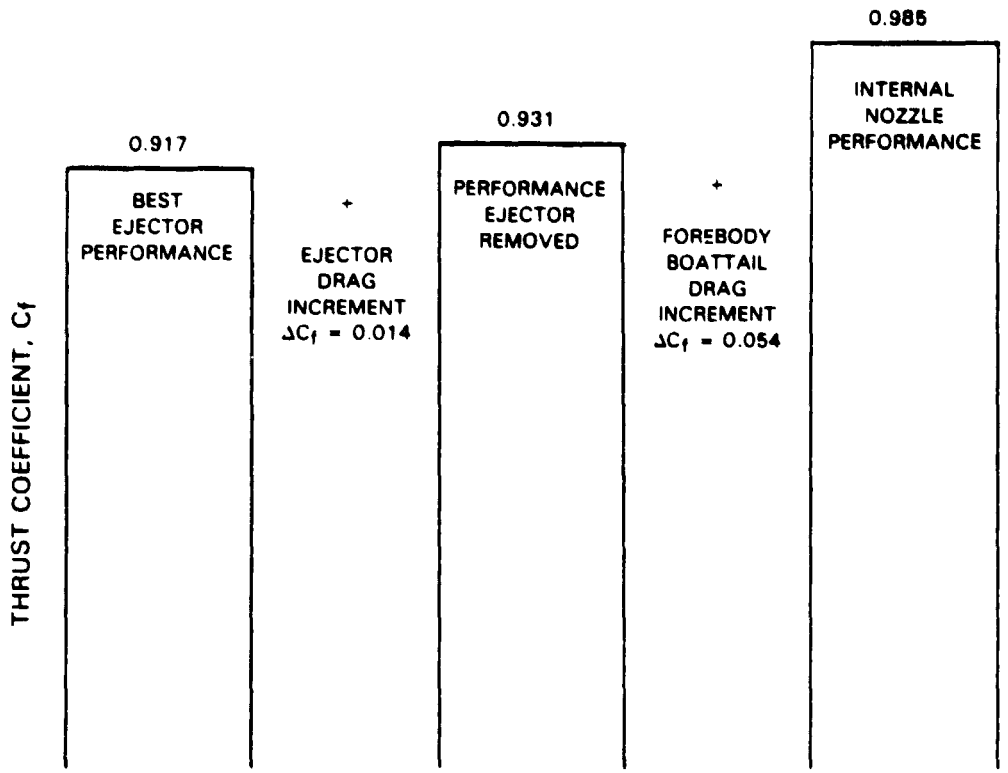

Figure 5.1-8 Internal Nozzle Performance Determined By Summing Ejector and Forebody Boattail Drag Increments, ΔC_f. Conditions: Forebody Boattail Angle, β, 14°; Freestream Mach Number, M_0, 0.9; Fan-to-Primary Pressure Split, P_{tf}/P_{tp}, 2.05; Fan Nozzle Pressure Ratio, P_{tf}/P_0, 5.09.

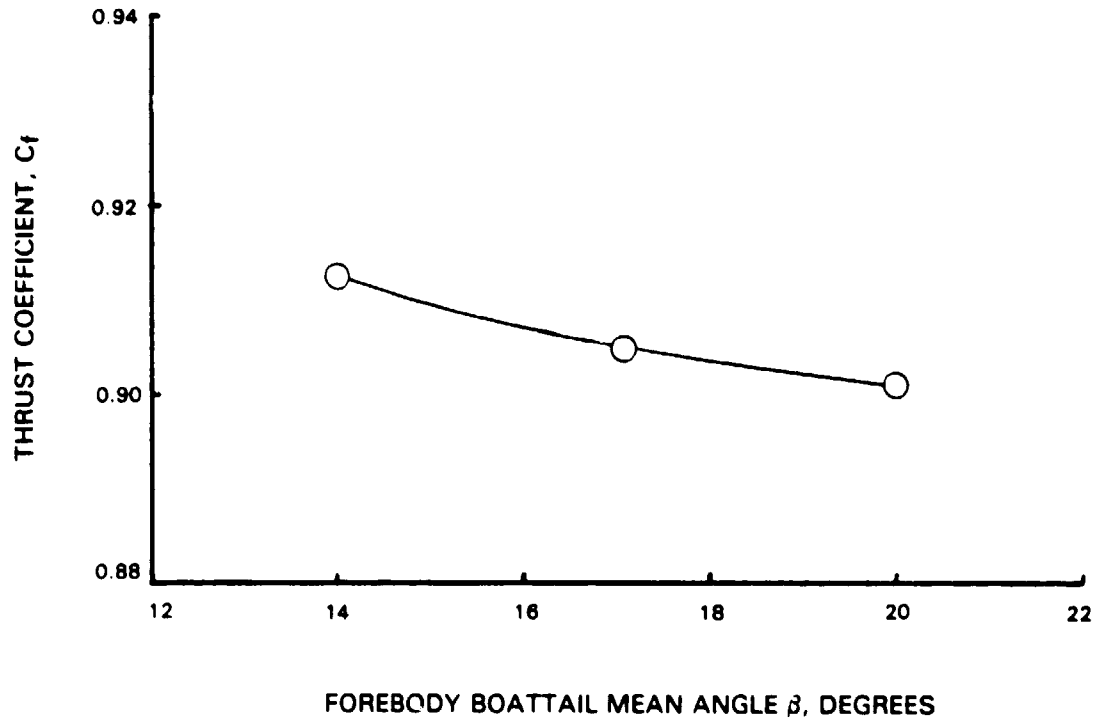

Figure 5.1-9 Effect of Forebody Boattail Angle, β, on Subsonic Cruise Nozzle Performance. Conditions: Freestream Mach Number, M_0, 0.9; Ejector Inlet and Exit Area Ratios, A_{in}/A_j, 1.0; A_{ex}/A_j, 2.04; Fan-to- Primary Pressure Split, P_{tf}/P_{tp}, 2.05; Fan Nozzle Pressure Ratio, P_{tf}/P_0, 5.09.

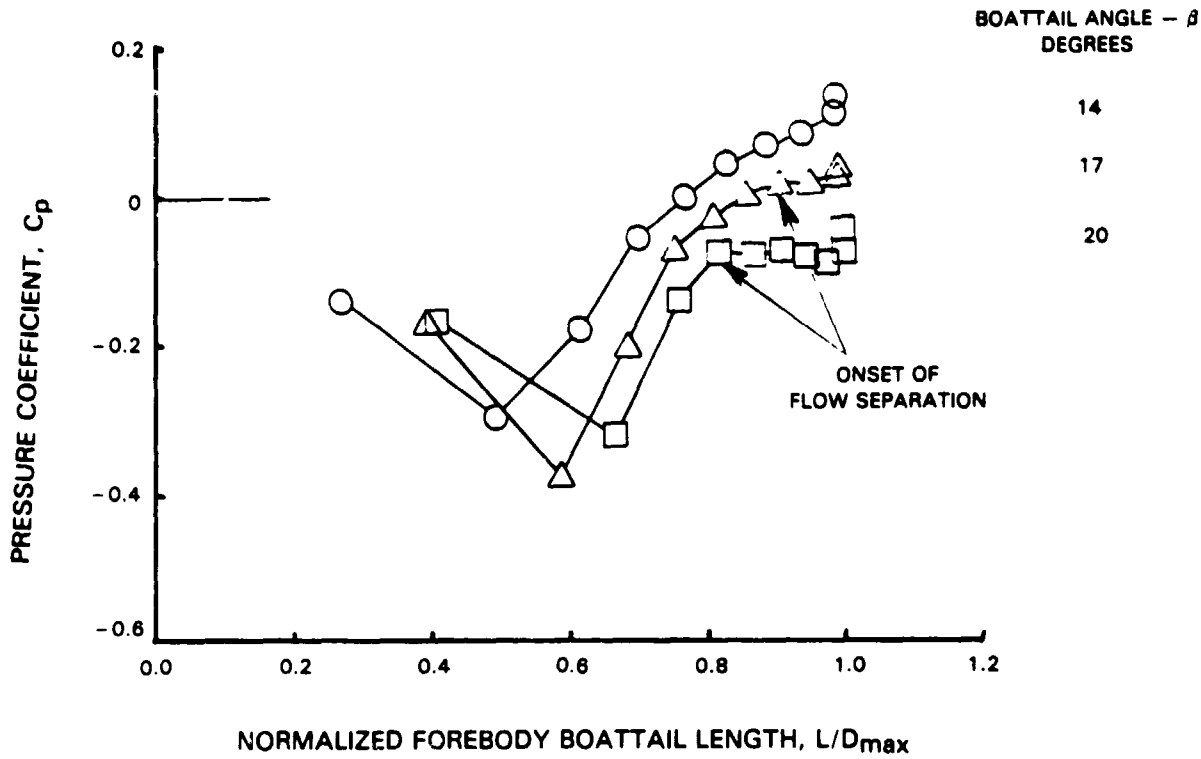

Figure 5.1-10 Forebody Boattail Pressure Distributions, C_p. Conditions: Freestream Mach Number, M_o, 0.9; Ejector Inlet and Exit Area Ratios, A_{in}/A_j, 1.0; A_{ex}/A_j, 2.04; Fan-to-Primary Pressure Split, P_{tf}/P_{tp}, 2.05; Fan Nozzle Pressure Ratio, P_{tf}/P_o, 5.09.

5.1.3 Transonic Cruise Performance

The influence of fan-to-primary pressure split, P_{tf}/P_{tp}, on transonic cruise thrust performance is shown in Figure 5.1-11 as a function of fan nozzle pressure ratio, P_{tf}/P_o. These data were acquired for the ejector inlet open configuration with the inlet area ratio, A_{in}/A_j, set at 0.63. A comparison of the three data sets shows that pressure split exerts a strong influence on performance, with thrust coefficient increasing with decreasing pressure split in a similar manner to the performance trend observed for the subsonic cruise configuration in Figure 5.1-3. The higher level of performance associated with decreasing pressure split is again explained by the reduction of internal over-expansion losses with increasing primary flow and by the increase in thrust at a constant fan nozzle pressure ratio while the external drag due to the freestream flow remains relatively constant.

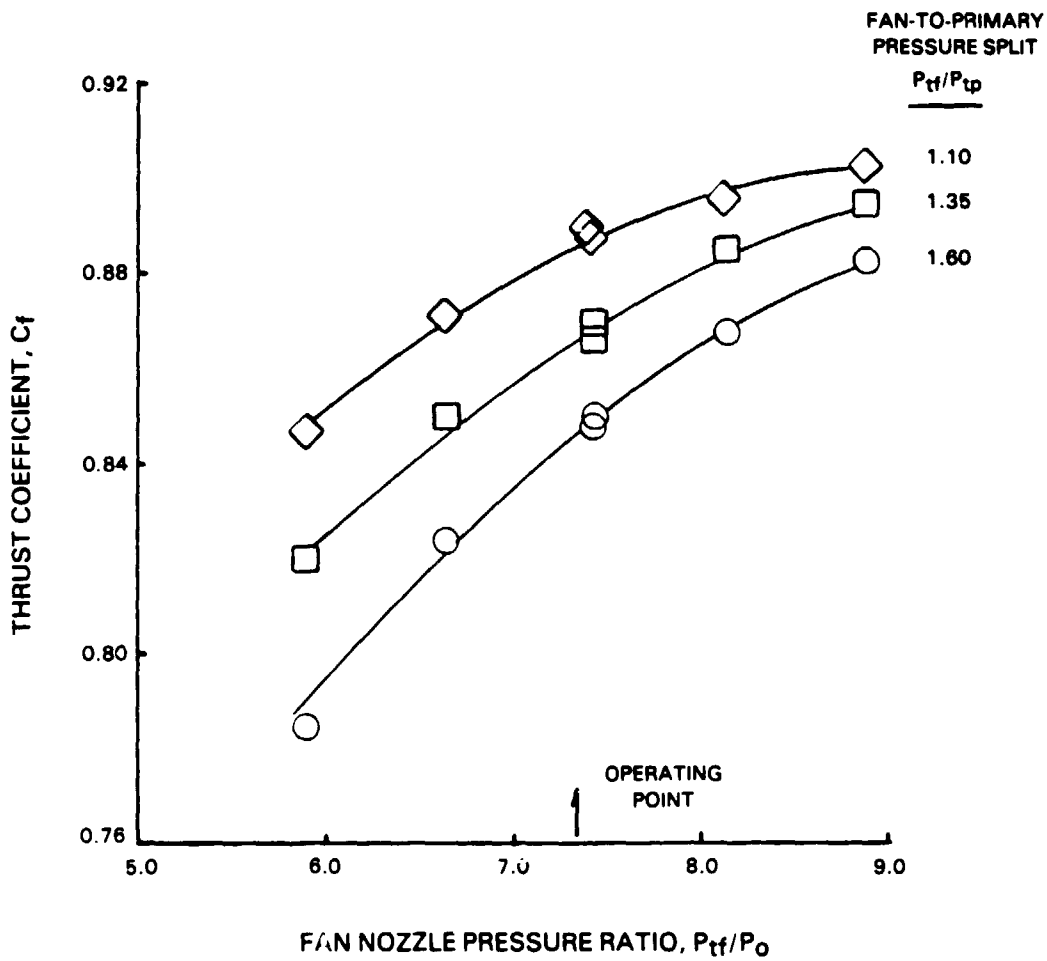

Figure 5.1-11 Influence of Fan-to-Primary Nozzle Pressure Split on Transonic Cruise Performance. Conditions: Freestream Mach Number, M_o, 1.2; Ejector Inlet Area Ratio, A_{in}/A_j, 0.63.

The effect of varying ejector inlet area, A_{in}/A_j, on transonic cruise performance is shown in Figure 5.1-12 at the nominal nozzle operating conditions. The constant level of thrust coefficient, a C_f of 0.866, shows that performance is insensitive to inlet area variation. Analysis of the static pressure distributions over the forebody boattail and ejector shroud internal surface, shown in Figure 5.1-13, reveals the 13.5° boattail has extensive flow separation in the region of the ejector inlet. The flow separation produces significant boattail base drag and reduces the effectiveness of the inlet flow in ventilating the ejector shroud.

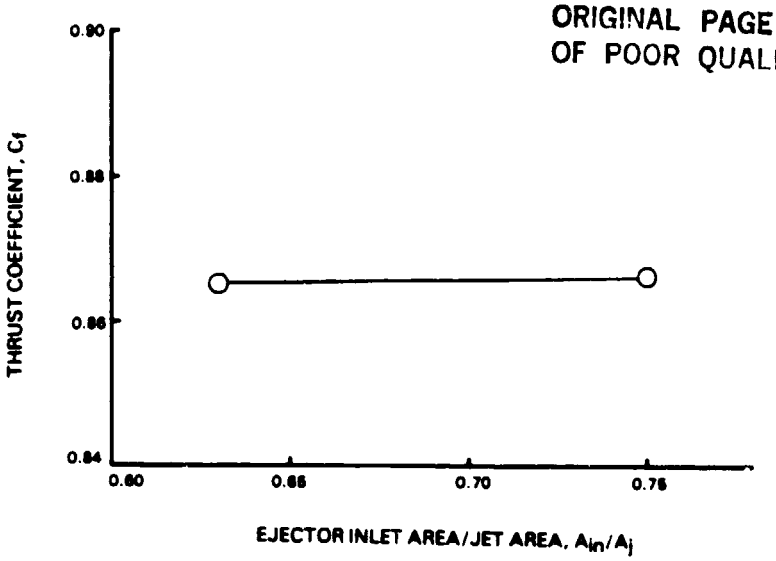

Figure 5.1-12 Influence of Ejector Inlet Area on Transonic Cruise, Performance. Conditions: Freestream Mach Number, M_0, 1.2; Fan-to-Primary Pressure Split, P_{tf}/P_{tp}, 1.35; Fan Nozzle Pressure Ratio, P_{tf}/P_0, 7.31.

Examination of the ejector shroud pressure distribution shows that some freestream flow is entering the inlet as indicated by the near stagnation pressure at the shroud leading edge, C_p=1.24. Inlet total pressure measurements would be required for a qualitative evaluation of the inlet flow losses. The rapid rise in shroud static pressure to a C_p = 0.96 at L/D_{max} of 1.25 indicates that a strong shock is occurring in the internal jet flow, resulting in an additional loss of nozzle thrust. The shock is believed to be emanating off the trailing edge of the flow splitter because of a static pressure mismatch between the merging fan and primary streams. The static pressure imbalance is a result of the low fan-to-primary total pressure split, P_{tf}/P_{tp} = 1.35, at the transonic cruise engine operating condition, whereas the flow splitter was designed for an engine pressure split of approximately 2.1 P_{tf}/P_{tp}, which occurs at subsonic and supersonic cruise operating conditions (refer to Table 3.2-I). The low level of performance for the transonic cruise configuration with the ejector inlet open is thus attributed to inlet flow losses, base drag and internal thrust losses.

Improved performance can be obtained by eliminating the inlet flow separation through a reduction of boattail angle and recontouring the ejector inlet. Refinement of the flow splitter geometry, increased axial separation of the fan and primary nozzle throats, to minimize the shock induced thrust loss will result in a further performance improvement.

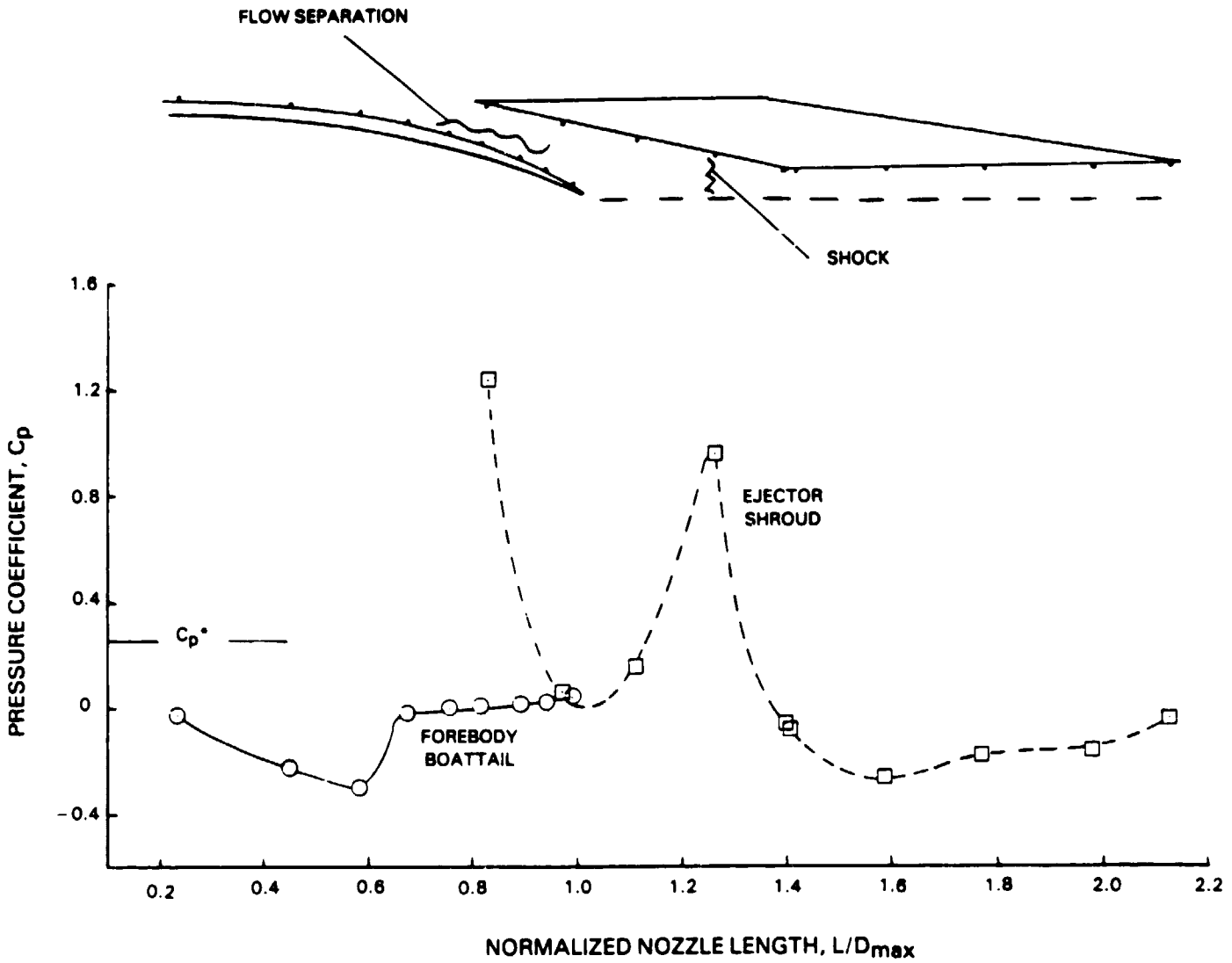

Figure 5.1-13 Static Pressure Distribution Over Forebody Boattail and Ejector Shroud Internal Surface. Conditions: Freestream Mach Number, M_o, 1.2; Ejector Inlet Area Ratio, A_{in}/A_j, 0.o3; Fan-to-Primary Pressure Split, P_{tf}/P_{tp}, 1.35; Fan Nozzle Pressure Ratio, P_{tf}/P_o, 7.4.

The effect of closing the ejector inlet at transonic cruise is presented in the performance comparison of Figure 5.1-14. At the nominal operating conditions, P_{tf}/P_0 = 7.31, the performance of ejector inlet closed configuration is one-half percent below that of the inlet open model. With the ejector closed, a loss in internal thrust performance resulted from over expansion of the nozzle flow, as shown by a plot of the shroud internal static pressure distribution presented in Figure 5.1-15. Analysis of these data shows that the static pressure of the expanding nozzle flow is dropping rapidly below ambient pressure, typical of a C-D nozzle operating over-expanded. At the ejector exit the flow is greatly over expanded, P1/Po = 0.35, resulting in a large internal thrust loss. The pressure distribution also shows a sudden static pressure rise at a shroud L/D_{max} of 1.3, indicating a strong shock in the nozzle flow. The second pressure rise seen at an L/D_{max} of 1.4 is associated with the abrupt flow turning created by the sharp intersection of the hinged shroud and tailfeather flaps. The shock, located at an L/Dmax of 1.3, is seen to occur at approximately the same shroud location (L/Dmax of 1.25) as was observed for the inlet open configuration in Figure 5.1-13. The similar location of the shock in both shrouds, inlet open and closed, further suggest the shock is emanating from the trailing edge of the flow splitter. Performance of the ejector inlet closed configuration can be improved by recontouring the flow splitter to minimize the shock induced thrust loss. Over-expansion thrust loss could be reduced by decreasing the shroud exit area, but at the expense of increased external drag due to a steeper flap angle. The optimum geometry would represent a tradeoff between the internal and external losses. Again it should be emphasized that the configuration was not designed to maximize transonic cruise performance. However, subsequent interest in transonic cruise operation led to the evaluation of the design in this flight regime.

5.1.4 Supersonic Cruise Performance

Supersonic cruise nozzle performance curves for the three fan-to-primary total pressure splits tested, P_{tf}/P_{tp}, are presented as a function of fan nozzle pressure ratio, P_{tf}/P_0, in Figure 5.1-16. Comparison of the three data sets shows that pressure split influences performance at the lower fan nozzle pressure ratios tested, but exhibits no effect at the engine operating point, P_{tf}/P_0 = 27.6. These results suggest that nozzle performance will not be degraded if engine operation deviates somewhat from the predicted pressure split of 2.12 at supersonic cruise. The reduced level of performance at the lower nozzle pressure ratios tested is again related to the over-expansion losses associated with a C-D nozzle operating at reduced pressure ratio. At higher fan nozzle pressure ratios in the region of nominal operating conditions, the nozzle flow is fully expanded and the maximum level of performance, C_f of 0.982, is achieved. Examination of the internal static pressure distribution measured along the ejector shroud at the nominal operating conditions (Figure 5.1-7) shows that the nozzle flow is fully expanded to ambient pressure at the shroud exit, P_1/P_0 = 1.0. The pressure distribution also shows a sudden rise in static pressure, P_1/P_0 = 2.3,

located at a shroud L/Dmax of 1.32, indicating the presence of a shock in the nozzle flow. The location of the shock on the shroud wall is similar to the shock location observed in the transonic cruise configuration ejector shrouds, refer to Figures 5.1-13 and 5.1-15, and is originating off the trailing edge of the flow splitter. Refinement of the splitter contour, previously discussed, to minimize the shock loss would result in an even higher level of supersonic cruise performance.

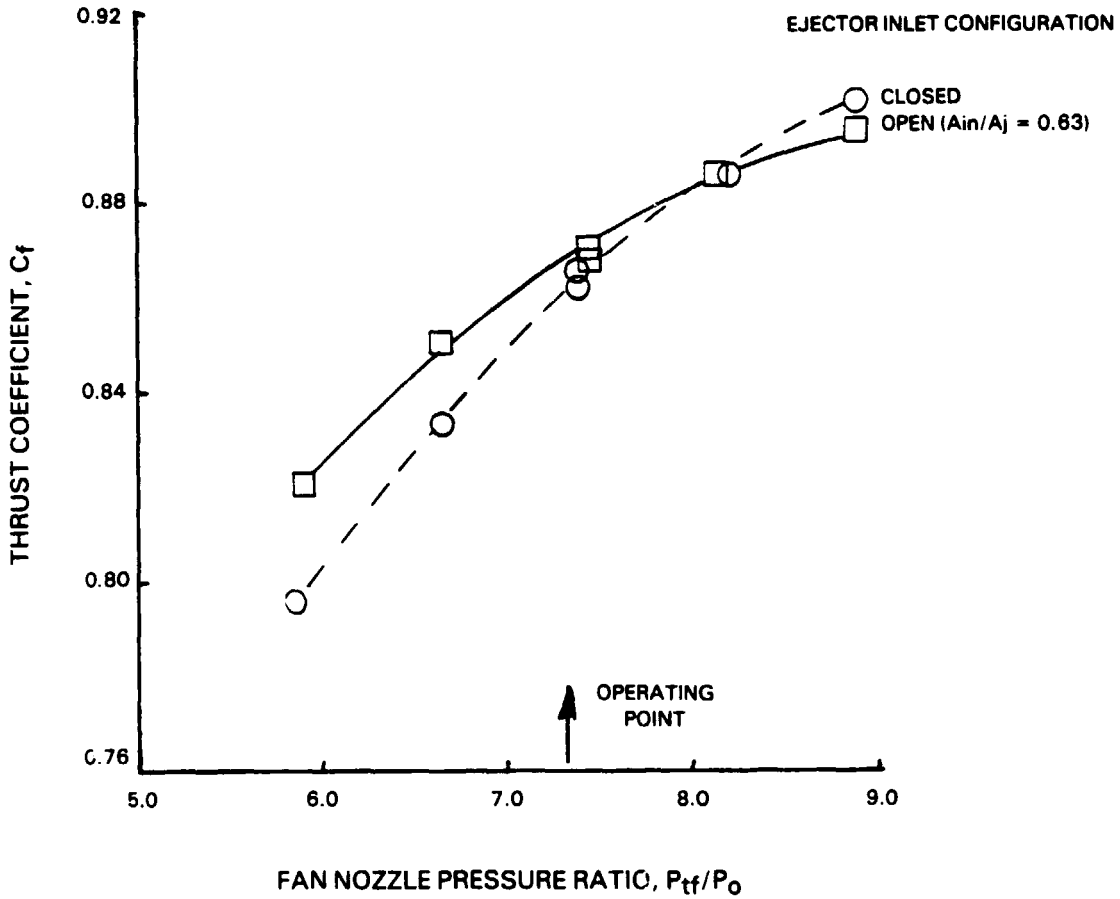

Figure 5.1-14 Comparison of Transonic Cruise Nozzle Performance With Ejector Inlet Open and Closed. Conditions: Freestream Mach Number, M_o, 1.2; Fan-to-Primary Pressure Split, P_{tf}/P_{tp}, 1.35; Fan Nozzle Pressure Ratio, P_{tf}/P_o, 7.4.

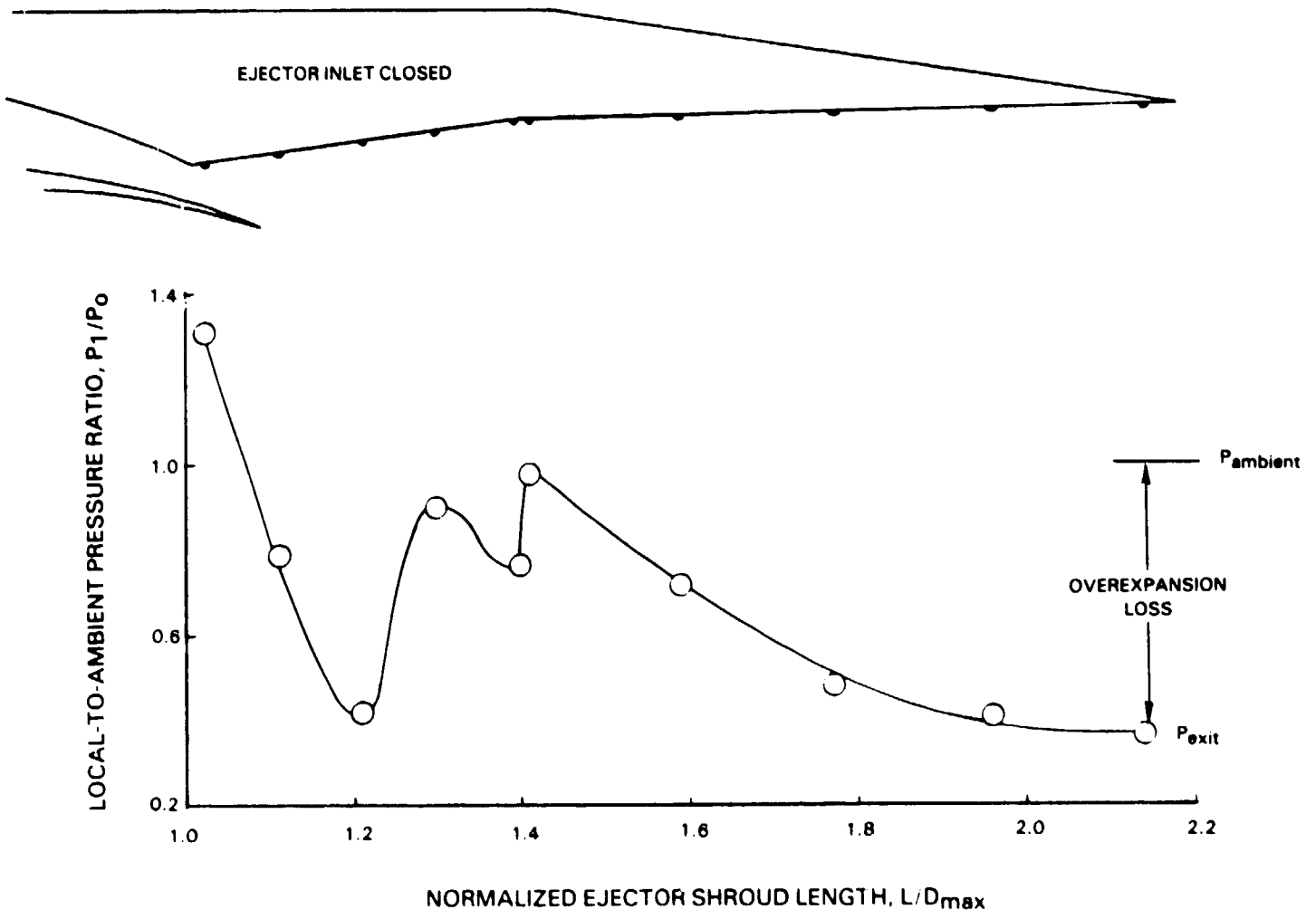

Figure 5.1-15 Static Pressure Distribution Over Ejector Shroud Internal Surface, Inlet Closed. Conditions: Freestream Mach Number, M_o, 1.2; Fan-to-Primary Pressure Split, P_{tf}/P_{tp}, 1.35; Fan Nozzle Pressure Ratio, P_{tf}/P_o, 7.4.

ORIGINAL PAGE IS
OF POOR QUALITY

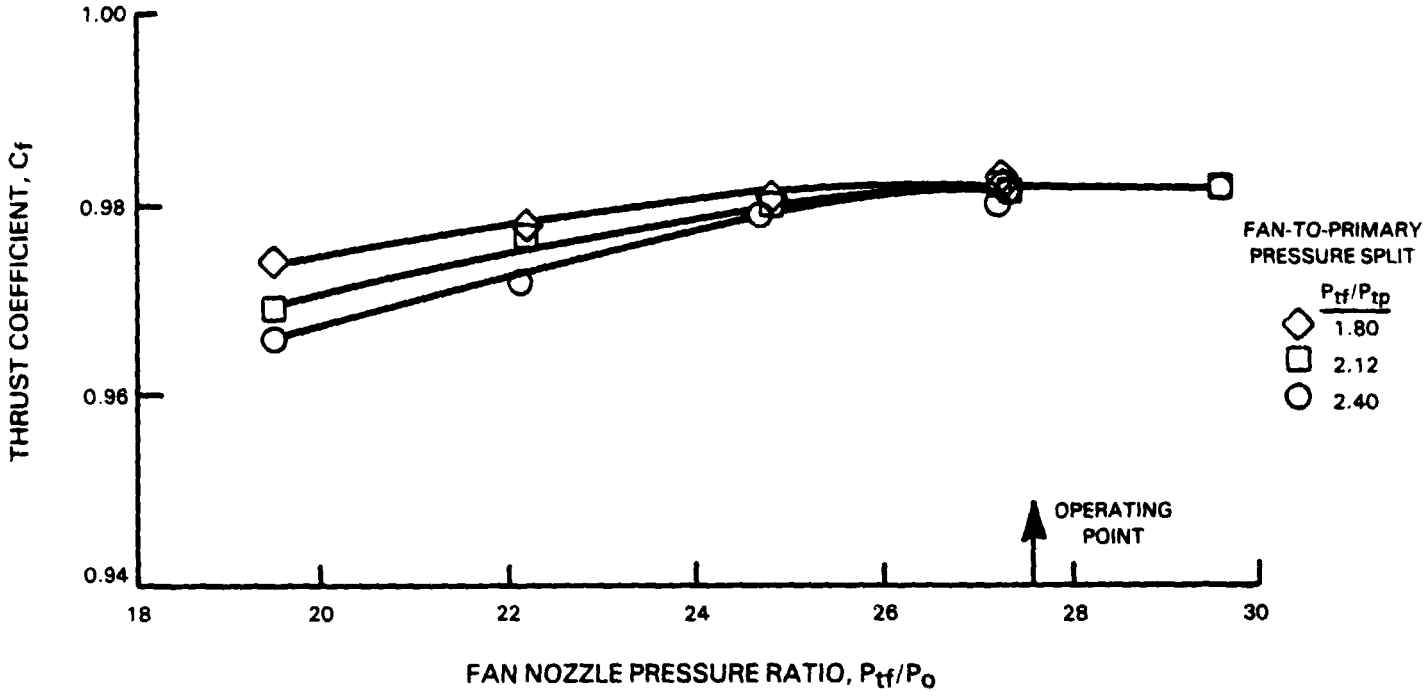

Figure 5.1-16 Influence of Fan-to-Primary Nozzle Pressure Split on Supersonic Cruise Performance. Condition: Freestream Mach Number, M_0, 2.0.

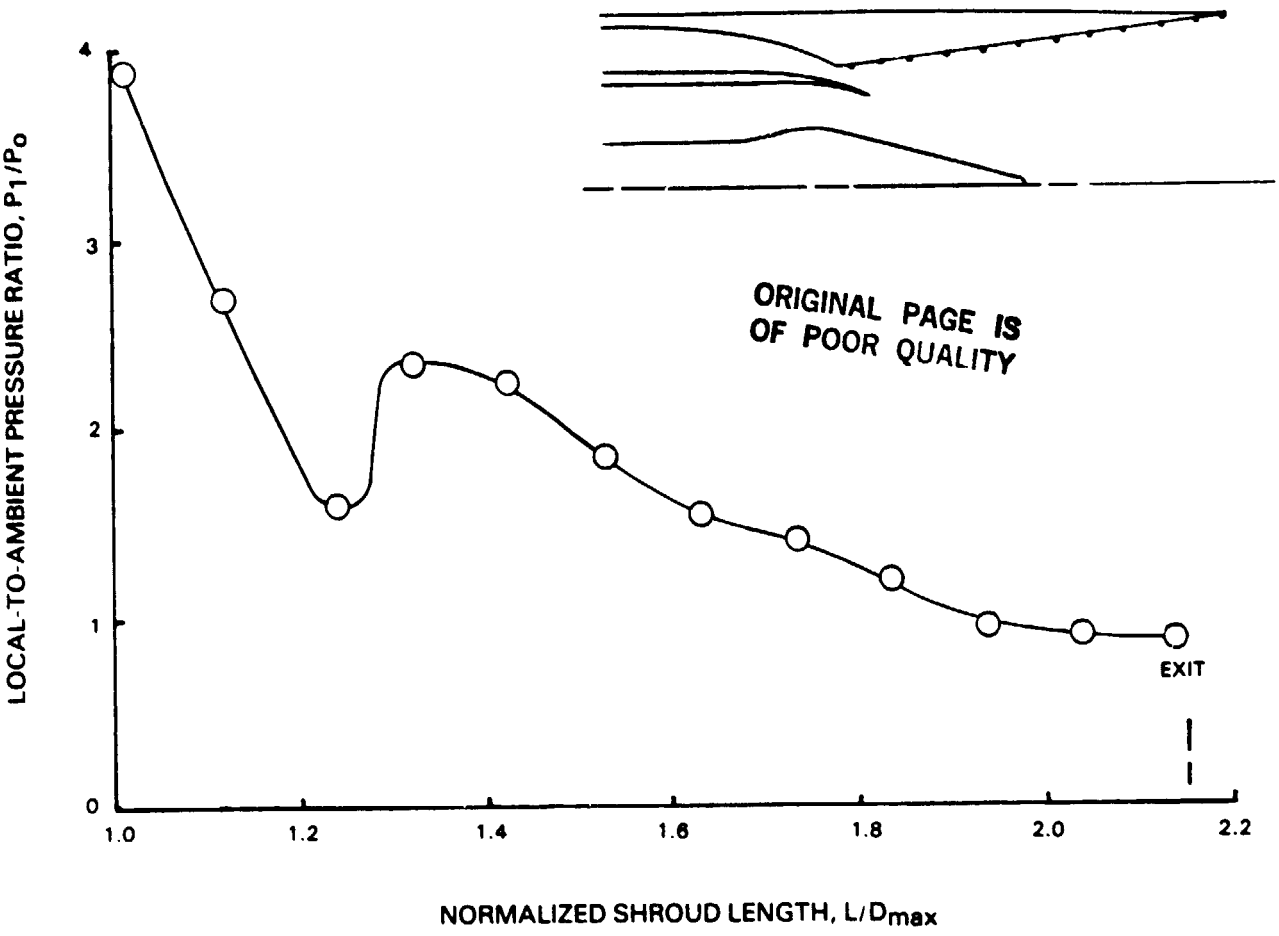

Figure 5.1-17 Supersonic Cruise Ejector Shroud Internal Static Pressure Distribution. Conditions: Freestream Mach Number, M_o, 2.0; Fan-to-Primary Pressure Split, P_{tf}/P_{tp}, 2.12; Fan Nozzle Pressure Ratio, P_{tf}/P_o, 27.3.

5.2 COMPARISON OF RESULTS TO PREVIOUS EJECTOR TESTS AND AST PROPULSION STUDY PERFORMANCE GOALS

Performance of the refined actuated inlet ejector nozzle is compared with the iris and short flap ejector nozzle configurations previously tested (Reference 5) at takeoff, subsonic and supersonic cruise in Figure 5.2-1. The comparisons are on the basis of performance at the predicted engine operation point for each flight condition. Relative to the iris nozzle which exhibited better takeoff and subsonic cruise performance, the refined design shows a takeoff performance improvement of 0.3 percent statically and 1.6 percent at fly-over conditions. At subsonic cruise, the refined design shows a significant 4.2 percent improvement in performance. At supersonic cruise, the comparison shows the refined configuration achieved the high level of nozzle performance previously demonstrated.

The comparison of test results with the performance goals established in the AST propulsion study shows that the takeoff performance goal was met at static conditions and nearly achieved, within 0.9 percent, at the Mo 0.36 fly-over condition. Subsonic cruise performance was within 2.3 percent of the goal. The comparison also shows that the critical supersonic cruise performance goal was attained.

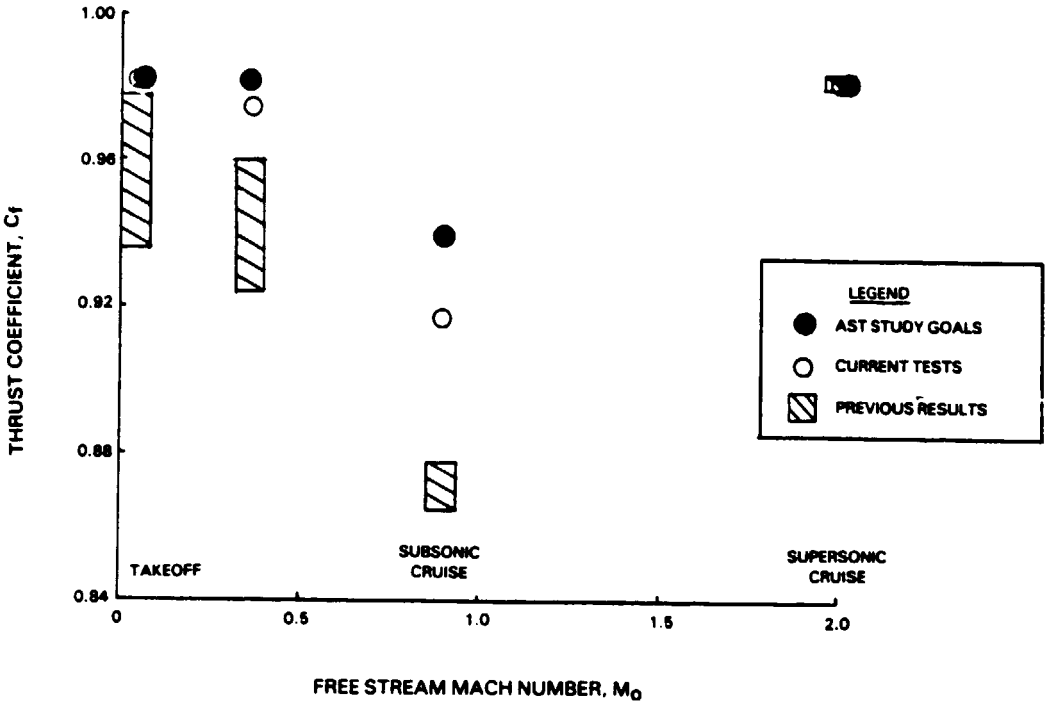

Figure 5.2-1 Comparison of Refined Actuated Inlet Ejector Nozzle Performance With Previous Ejector Test Results and AST Propulsion Study Performance Goals.

5.3 NOZZLE FLOW COEFFICIENTS

5.3.1 Takeoff Configuration Flow Coefficients

Takeoff configuration fan nozzle flow coefficients are compared at quiescent and Mo 0.36 fly-over conditions for the range of fan-to-primary total pressure splits tested in Figure 5.3-1. The collapse of the data compared shows that the fan nozzle flow coefficient is not affected by pressure split, P_{tf}/P_{tp}, nor freestream flow effects at the nominal operating point, P_{tf}/P_o of 2.84. The data exhibit a conventional trend with decreasing nozzle pressure ratio, tending to decrease slightly at near sonic flow

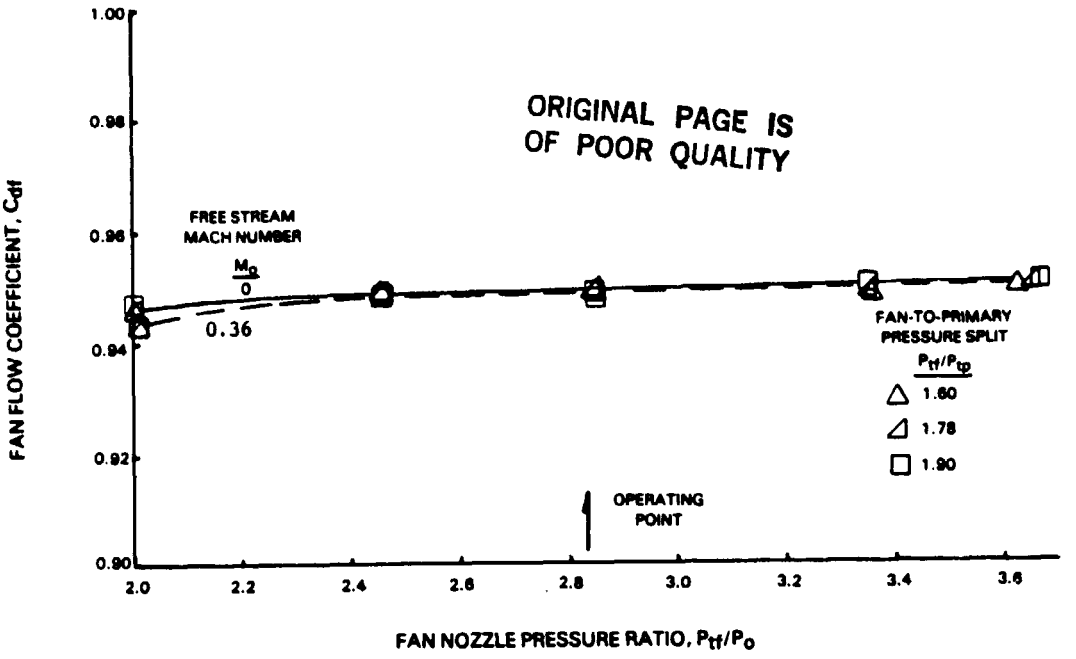

Figure 5.3-1 Comparison of Takeoff Configuration Fan Nozzle Flow Coefficients at Quiescent and M_0 = 0.36 Freestream Conditions. Ejector Inlet and Exit Area Ratio: A_{in}/A_j, 0.87, A_{ex}/A_j, 1.60.

conditions. Here it can be seen at a fan nozzle pressure ratio of 2.0 that the freestream flow causes a one-half percent decrease in fan nozzle flow coefficient.

Primary nozzle flow coefficients measured at quiescent operating conditions fall off significantly with decreasing primary nozzle pressure ratio, P_{tp}/P_0, as seen in Figure 5.3-2a. These data also show that the fall off rate is influenced by fan-to-primary pressure split, P_{tf}/P_{tp}, at nozzle pressure ratios less than 2.0. The decrease in flow coefficient, Cdp, below a P_{tf}/P_0 of 2.0 is explained by the flow choking phenomena. As primary nozzle pressure ratio decreases below 2.0, the primary flow unchokes and is suppressed by the surrounding fan exhaust flow. At primary pressure ratios greater than 2.0, the collapse of the data to a constant level indicates choked-nozzle operation and that the fan stream has no influence. At the nominal takeoff operating conditions, P_{tf}/P_0 = 1.6, there is a 3.5 percent variation in primary flow coefficient over the range of pressure splits tested. A comparison of primary flow coefficients at static and Mo 0.36 fly-over conditions for the nominal fan-to-primary pressure split, P_{tf}/P_{fp} = 1.78, is presented in Figure 5.3-2b. The comparison shows that the freestream flow causes an eight percent decrease in primary nozzle flow coefficient relative to static operation at the nominal engine operating point, P_{tf}/P_0 = 1.6. This reduction in primary flow at fly-over conditions can be overcome by retracting the primary plug to increase the nozzle flow area if required.

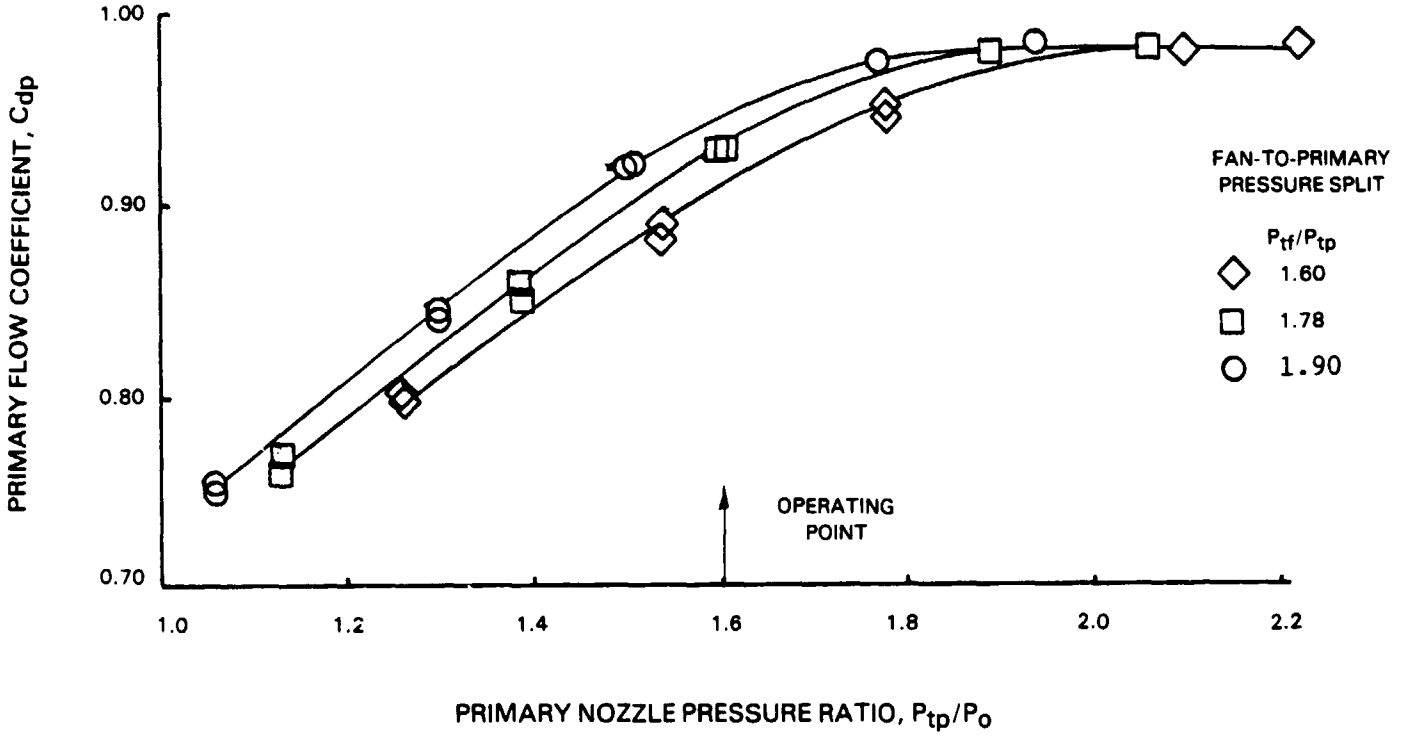

(a) Influence of Fan-to-Primary Pressure Split on Flow Coefficient. Condition: Freestream Mach Number, M_o,=0.

Figure 5.3-2 Takeoff Configuration Primary Nozzle Flow Coefficients. Ejector Inlet and Exit Area Ratio, A_{in}/A_j, 0.87; A_{ex}/A_j, 1.60.

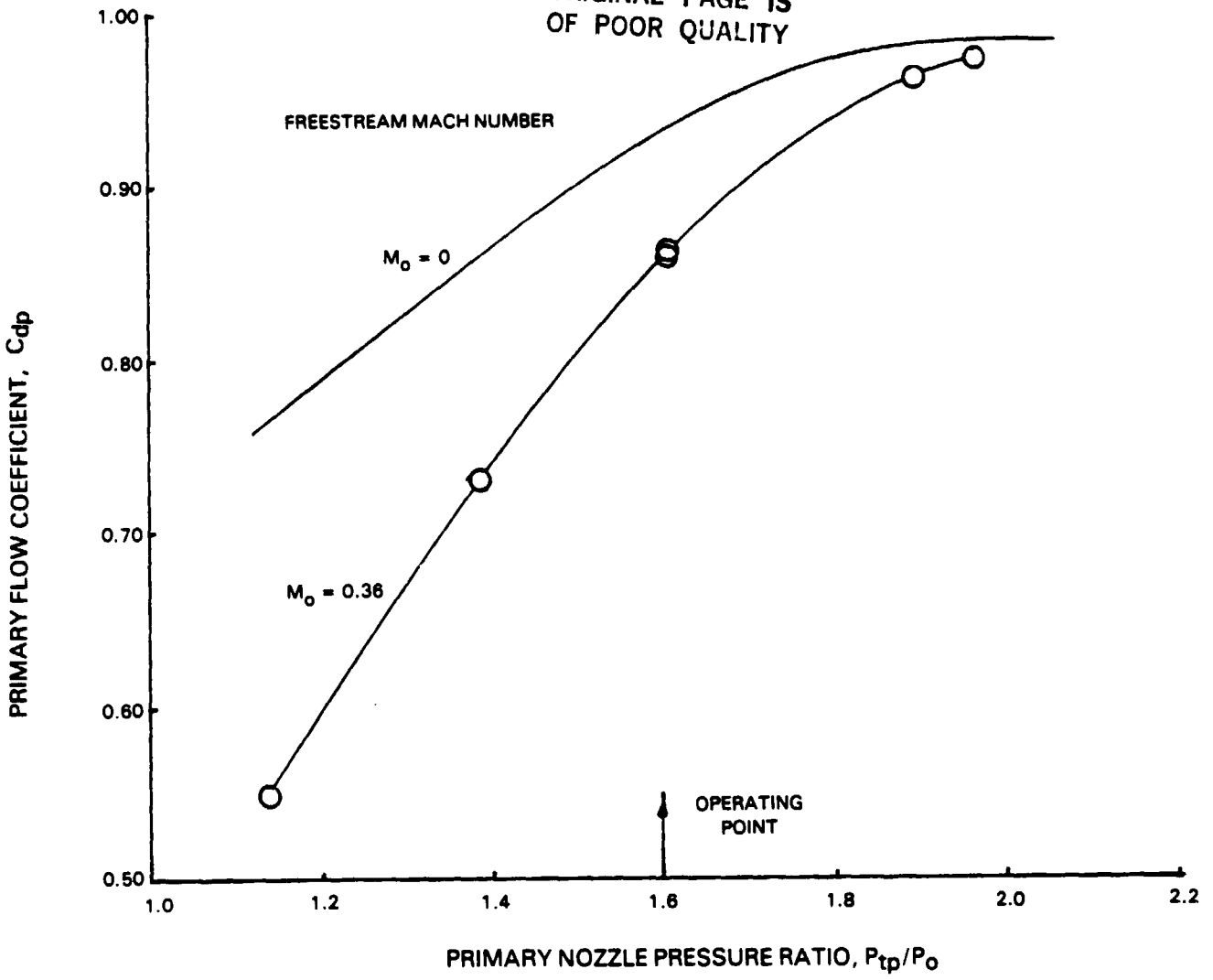

(b) Comparison of Flow Coefficient at Quiescent and M_o = 0.36 Freestream Condition. Condition: Fan-to-Primary Pressure Split, P_{tf}/P_{tp}, 1.78.

Figure 5.3-2 Takeoff Configuration Primary Nozzle Flow Coefficients. Ejector Inlet and Exit Area Ratio, A_{in}/A_j, 0.87; A_{ex}/A_j, 1.60. (Concluded)

At the nominal nozzle operating conditions, the level of fan nozzle flow coefficient for both quiescent and Mo 0.36 fly-over conditions is 0.949. The level of the primary flow coefficient is 0.930 statically and 0.853 at 0.36 Mo.

5.3.2 Subsonic Cruise Configuration Flow Coefficients

Fan and primary nozzle flow coefficients obtained with the 14° forebody boattail subsonic cruise configuration, tested at 0.9 Mo, are presented in Figure 5.3-3. For each plot, data are presented at the three fan-to-primary pressure splits tested. Collapse of the fan nozzle data, Figure 5.3-3a, to a constant value shows the fan nozzle flow coefficient is independent of nozzle operating conditions over the range tested. The linear trend of fan nozzle flow coefficient as a function of nozzle pressure ratio, P_{tf}/P_o, is characteristic of choked nozzle operation.

Examination of the primary nozzle flow coefficient data, Figure 5.3-3b, shows that the primary nozzle flow begins to unchoke below a primary pressure ratio of 2.6 and decreases rapidly with decreasing pressure ratio, P_{tf}/P_o, and to a lesser extent with pressure split, P_{tf}/P_{tp}. Unchoked operation at nozzle pressure ratios above critical indicates that the local exit pressure is greater than ambient. Impingment of the strong supersonic fan stream on the primary flow produces this result. At the nominal operating point, a P_{tf}/P_o of 2.48, the level of flow coefficient is slightly reduced, 0.5 to 1.0 percent, relative to the choked level at a pressure split of 1.8. At the nominal nozzle operating conditions, P_{tf}/P_{tp} of 2.05 and P_{tf}/P_o of 5.09, the level of fan and primary nozzle flow coefficients are Cdf = 0.926 and Cdp = 0.980.

5.3.3 Transonic Cruise Configuration Flow Coefficients

Fan and primary nozzle flow coefficients for the transonic cruise configurations tested with the ejector inlet open and closed are presented in Figure 5.3-4 as a function of fan nozzle pressure ratio, P_{tf}/P_o. Fan and primary flow coefficients of both configurations exhibit a choked flow characteristic as would be expected with nozzle operating conditions, P_{tf}/P_o from 5.9 to 8.9, well above the sonic flow regime. At the nominal nozzle operating conditions, a P_{tf}/P_o of 7.31 and P_{tf}/P_{tp} of 1.35, the levels of fan and primary nozzle flow coefficient for the ejector open configuration, Figure 5.3-4a are a Cdf of 0.942 and Cdp of 0.990; for the ejector closed configuration, Figure 5.3-4b, Cdf = 0.975 and Cdp = 0.990.

5.3.4 Supersonic Cruise Configuration Flow Coefficients

Fan and primary nozzle flow coefficients for the supersonic cruise configuration are presented in Figure 5.3-5 as a function of fan nozzle pressure ratio, P_{tf}/P_o. At the high nozzle pressure ratios associated with the supersonic cruise test conditions, P_{tf}/P_o from 19.5 to 29.6, the trend of both fan and primary nozzle flow coefficient is consistent with choked nozzle operation. At the nominal nozzle operating conditions, a P_{tf}/P_o of 27.6 and P_{tf}/P_{tp} of 2.12, the levels of fan and primary nozzle flow coefficient are 0.965 Cdf and 0.990 Cdp, respectively.

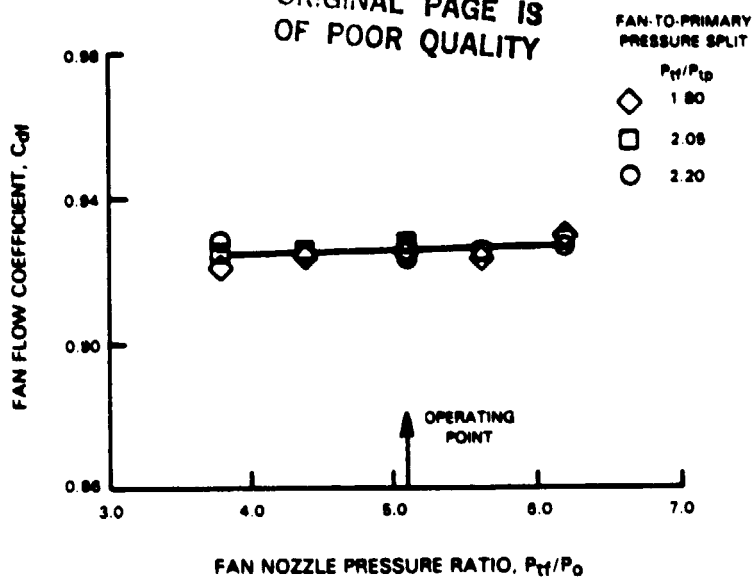

(a) Fan Nozzle Flow Coefficient

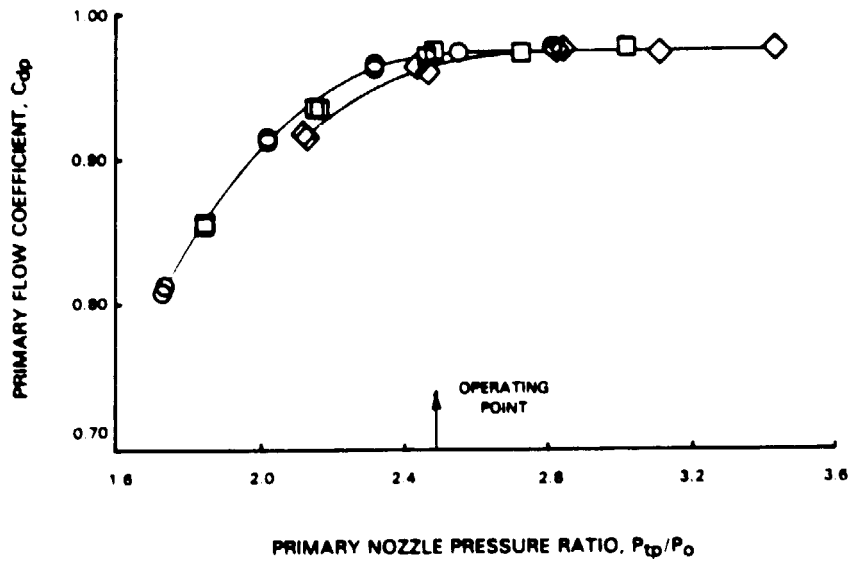

(b) Influence of Fan-to-Primary Pressure Split on Primary Nozzle Flow Coefficient

Figure 5.3-3 Subsonic Configuration Flow Coefficients. Conditions: Freestream Mach Number, M_o, 0.9; Forebody Boattail Angle, β, 14°; Ejector Inlet and Exit Area Ratio, A_{in}/A_j, 0.82; A_{ex}/A_j, 1.90.

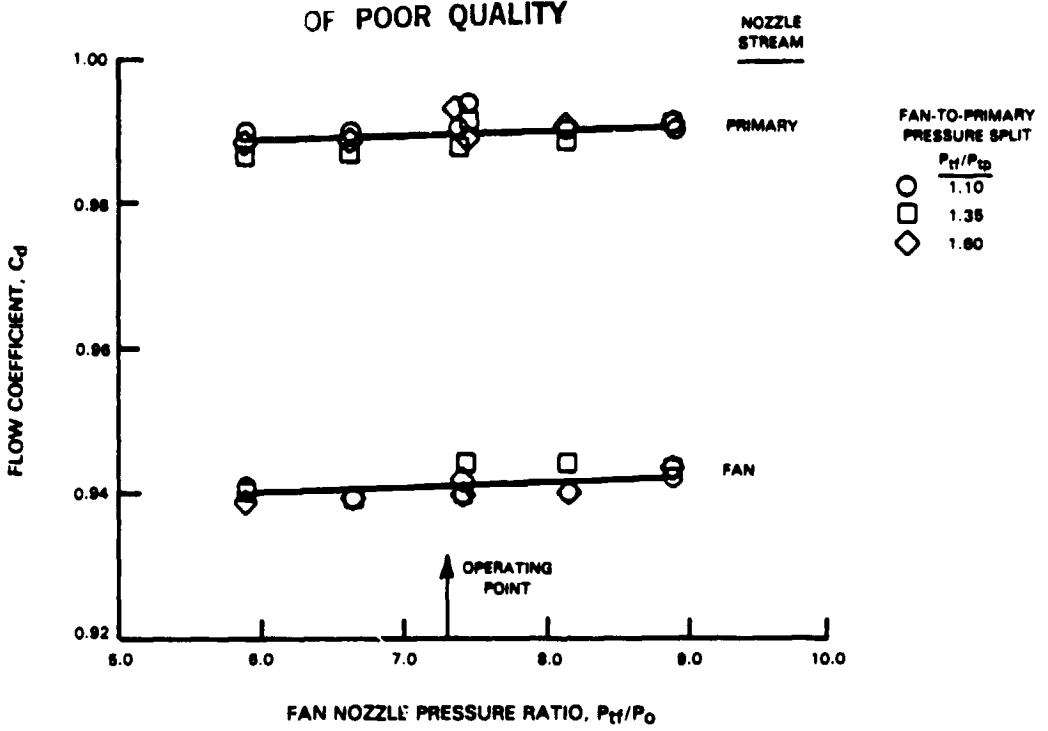

(a) Ejector Open Configuration. Ejector Inlet Area Ratio, A_{in}/A_j, 0.63.

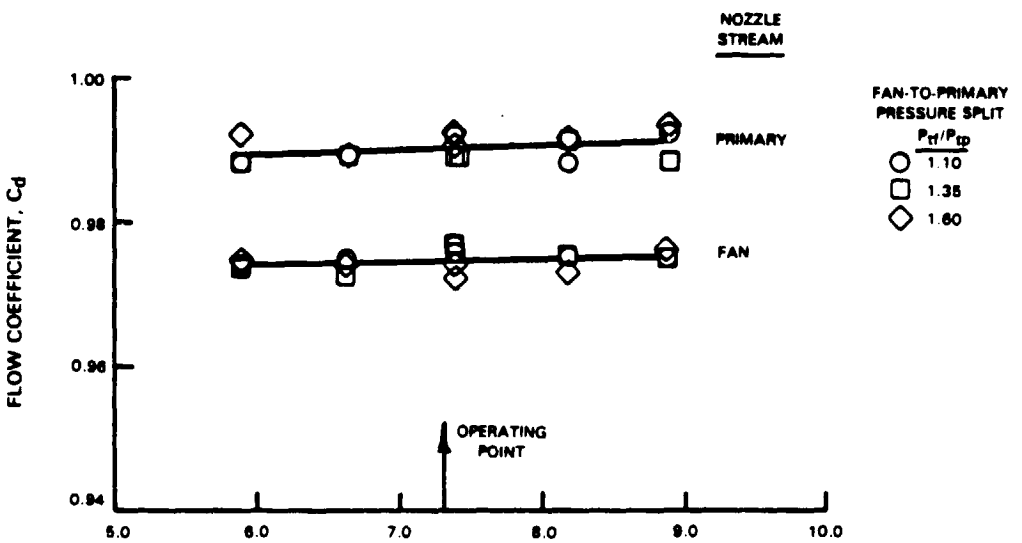

(b) Ejector Closed Configuration

Figure 5.3-4 Transonic Cruise Configuration Flow Coefficients. Condition: Freestream Mach Number, M_o, 1.2.

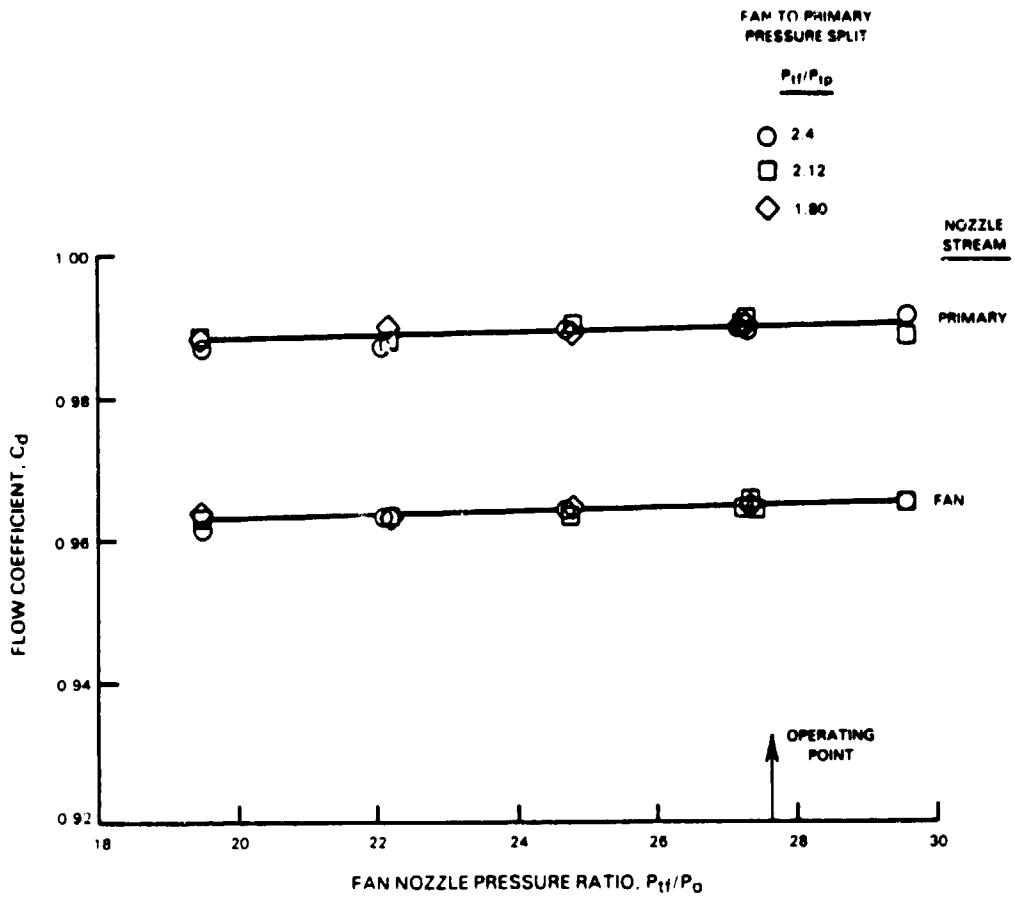

Figure 5.3-5 Supersonic Cruise Configuration Flow Coefficients. Conditions: Freestream Mach Number, M_0, 2.0.

SECTION 6.0

CONCLUSIONS

The major conclusions from the study are:

- The refined actuated inlet ejector nozzle demonstrated significant improvements in takeoff and subsonic cruise performance over the previous ejector nozzles tested. A comparable level of supersonic cruise performance was attained.
- The AST propulsion study performance goals were met at takeoff and supersonic cruise; subsonic cruise performance was within 2.3% of the goal.
- Transonic cruise performance was checked for two modes of ejector operation.

The significant results of the tests at engine operating conditions are summarized in the following sections.

6.1 TAKEOFF RESULTS

Maximum static performance at C_f of 0.983 was obtained with the ejector shroud configured at the smallest exit area and largest inlet area tested. Relative to the previous nozzle tests, static performance was improved 0.3 percent. Maximum fly-over performance at C_f of 0.974 occurred over a range of ejector inlet areas and the smallest shroud exit area tested. Relative to the previous nozzle test fly-over, performance was improved 1.6 percent.

6.2 SUBSONIC CRUISE RESULTS

Maximum subsonic cruise performance was obtained with the 14° boattail and the smallest ejector inlet and exit area tested. Performance increased with decreasing fan-to-primary pressure split: a C_f of 0.917 at the engine operating point and 0.923 at the minimum pressure split tested. Steeper boattail angles decreased performance. Tests with the ejector shroud removed showed that performance could be improved up to 0.9 percent by refining shroud design. A reduction of forebody boattail angle should yield further improvements. Decreased inlet and exit area may also improve performance. Relative to the previous test configurations, subsonic cruise performance was improved 4.2%.

6.3 TRANSONIC CRUISE RESULTS

Performance of the ejector inlet open configuration yielded a C_f of 0.866, and the ejector closed configuration was one-half percent less. The low levels of performance were due to inlet flow separation, internal shock, and over-expansion thrust losses. Performance can be improved by a reduction of boattail angle and refinements of the flow splitter and shroud design.

6.4 SUPERSONIC CRUISE PERFORMANCE

Good supersonic cruise performance was demonstrated at C_f of 0.982. Further improvements may be possible by refining the flow splitter geometry.

6.5 FACILITY VERIFICATION

STA nozzle results indicate that the measured internal thrust coefficients were lower than predicted at all but the supersonic cruise condition and suggest that the unadjusted thrust performance of the ejector nozzle research models presented herein is somewhat conservative at freestream Mach numbers of 0, 0.36, 0.9, and 1.2.

REFERENCES

1. Howlett, R. A. and Hunt, R. B., "VSCE Technology Definition Study," NASA Cr-159730, 1979.

2. Kozlowski, H. and Packman, A. B., "Aero/Acoustic Tests of Duct Burning Turbofan Nozzles," NASA CR-2628, 1976.

3. Kozlowski, H., and Packman, A. B., "Flight Effects of the Aero/Acoustic Characteristics of Inverted Velocity Profile Coannular Nozzles," NASA CR-3018, 1978.

4. Larson, R. S., Nelson, D. P., and Stevens, B. S., "Aerodynamic and Acoustic Investigation of Inverted Velocity Profile Coannular Exhaust Nozzle Models and development of Aerodynamic and Acoustic Prediction Procedures," NASA CR-3168, 1979.

5. Nelson, D. P., "Model Aerodynamic Test Results for Two Variable Cycle Engine Coannular Exhaust Systems at Takeoff and Cruise Conditions," NASA CR-159818, 1980.

6. Hunt, R. B. and Kardas, G. E., "Supersonic Cruise Nozzle Exhaust Systems: An Aeromechanical Design Study and Improvements to Analytical Techniques," NASA CR-165416, 1981.

7. Preliminary Design Boeing Commercial Airplane Company, "Large Payload Capacity SST Concepts - Technical and Economic Feasibility," NASA CR-165934, 1981.

8. Nelson, D. P., "Model Aerodynamic Test Results for a Refined Actuated Inlet Ejector Nozzle at Simulated Takeoff and Cruise Conditions, Comprehensive Data Report," NASA CR-168052, 1983.

9. Swallow, Robert J., and Aiello, Robert A., "NASA Lewis 8 by 6 Foot Supersonic Wind Tunnel," NASA TM X-71542, May 1974.

10. Johnson, R. C., "Real-Gas Effects in Critical Flow Through Nozzles and Tabulated Thermodynamic Properties," NASA TN D-2565, 1965.

11. Smith, K. D., "Methods and Charts for Estimating Skin Friction drag in Wind Tunnel Tests with Zero Heat Transfer," C.P. No. 824, Great Britain, 1965.

12. Staid, Paul S., "Wind Tunnel Performance Tests of Coannular Plug Nozzles," NASA CR 2990, 1978.

APPENDIX A

FACILITY VERIFICATION

A modified Supersonic Tunnel Association nozzle was constructed for this program and tested as a means of verifying the force and weight-flow measurement accuracy of the facility. The procedure and results are discussed in this Appendix.

Calibration Model Description

The geometric details of the modified Supersonic Tunnel Association (STA) nozzle are shown in Figure A-1. This nozzle is essentially an American Society of Mechanical Engineers (ASME) Standard nozzle with a base. The modified STA nozzle installation is shown in Figure A-2. Testing with this nozzle was conducted with both the fan flow (Wf) and primary flow (Wp) flowing simultaneously. Flow conditioning was provided by means of perforated "choke" plates and screens upstream of the nozzle. Nozzle total pressure was measured by two four-tube rakes, while nozzle total temperature was measured with two chromel-alumel thermocouples. Base static pressure was determined using four rows of six taps.

Calibration Model Data Reduction

In order to compare the modified Supersonic Tunnel Association nozzle thrust coefficients with semiempirical predicted levels, it was necessary to modify the thrust coefficient (C_f) as defined by equation 14 to account for the nozzle base drag, D_B

$$C_{f,int} = \frac{F - D_{ex}}{mV_i} + \frac{D_B}{mV_i} \tag{1A}$$

or

$$C_{f,int} = C_f + \Delta C_{fB} \tag{2A}$$

where C_f is the nozzle thrust coefficient corrected for friction drag as previously defined, D_B is the nozzle base drag as measured by twenty-four static pressure taps over the base area.

Calibration Model Results

Flow coefficients, stream thrust parameters and internal thrust coefficients for the modified Supersonic Tunnel Association nozzle are presented in Figures A-3 to A-5. Data were obtained as quiescent conditions and at Mach numbers of 0.36, 0.9 and 2.0. Testing was conducted by flowing air simultaneously from

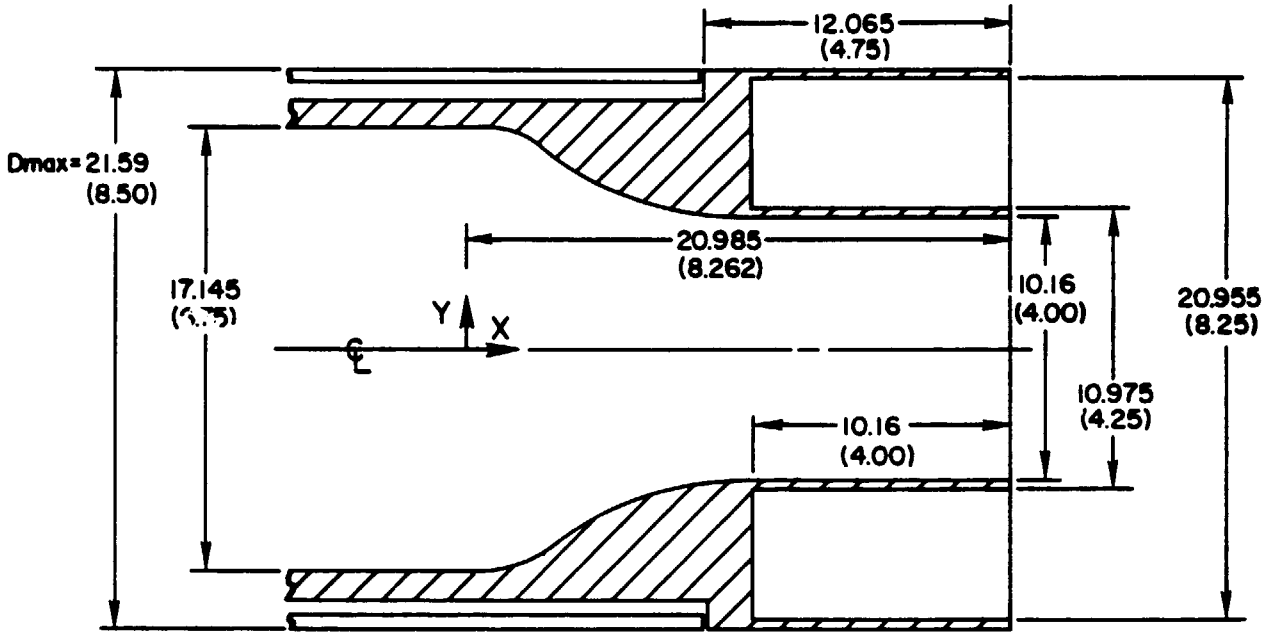

Nozzle Internal Coordinates

X Coordinates		Y Coordinates		
cm	in	cm	in	
0	(0)	8.573	(3.375)	Circular
0.665	(0.262)	8.529	(3.358)	
1.300	(0.512)	8.402	(3.308)	
1.935	(0.752)	8.189	(3.224)	
2.570	(1.012)	7.877	(3.101)	Elliptical
3.205	(1.252)	7.351	(2.894)	
3.840	(1.512)	5.915	(2.723)	
4.479	(1.762)	5.551	(2.579)	
5.110	(2.012)	5.241	(2.457)	
5.745	(2.252)	5.979	(2.354)	
5.380	(2.512)	5.755	(2.255)	
7.015	(2.752)	5.570	(2.193)	
7.550	(3.012)	5.415	(2.132)	
8.285	(3.252)	5.293	(2.084)	
8.920	(3.512)	5.199	(2.047)	
9.555	(3.752)	5.133	(2.021)	
10.190	(4.012)	5.093	(2.005)	
10.825	(4.252)	5.080	(2.000)	Cylindrical
20.985	(8.252)	5.080	(2.000)	

Figure A-1 Geometric Details of Modified Supersonic Tunnel Association (STA) Nozzle.

the fan and primary supply systems. The majority of the data shown were obtained using a 1.3015 inch diameter fan flow measuring venturi and a 1.299 inch diameter primary flow measuring venturi. The predicted levels of flow coefficient, stream thrust parameter and internal thrust coefficient were derived from semiempirical methods of calculating standard ASME long radius nozzle performance, as described in Reference 12.

The ASME equations were slightly modified to include the effect of a small difference in length of the internal flowpaths between the ASME and modified STA nozzles. The flow coefficients were well within + 0.5 percent of predicted levels for all the tested Mach numbers as shown in Figure A-3 indicating accurate flow measurements. The stream thrust parameter at the supersonic cruise Mach number of 2.0 also fell within + 0.5 percent of the predicted level. At the lower Mach numbers, however, there was a downward shift of 0.50 to 1.0 percent from the predicted level as shown in Figure A-4, indicating low load cell readings. For this reason the internal thrust coefficient also shifted 0.5 to 1.0 percent below the predicted levels for the corresponding Mach numbers, Figure A-5.

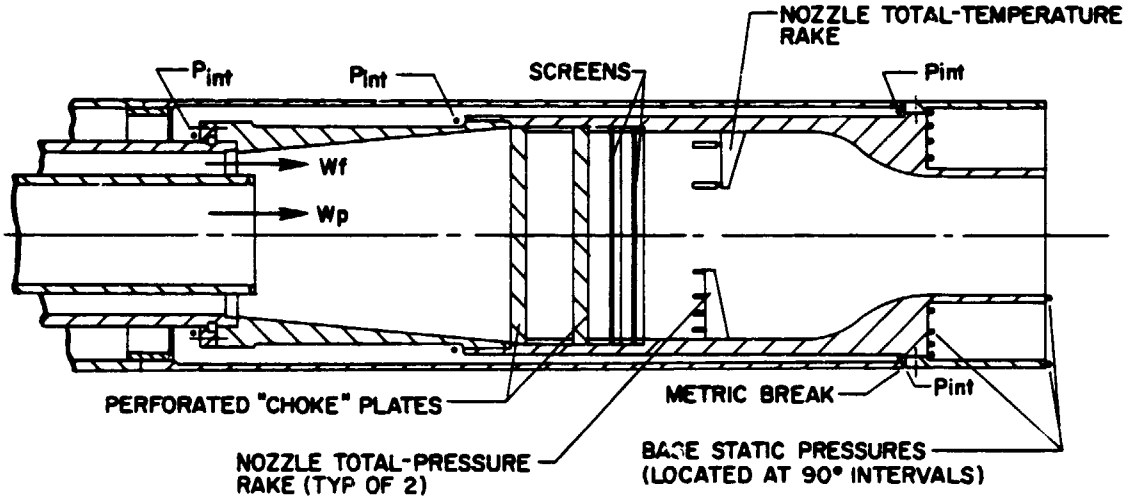

Figure A-2 Details of Modified Supersonic Tunnel Association Nozzle Installation

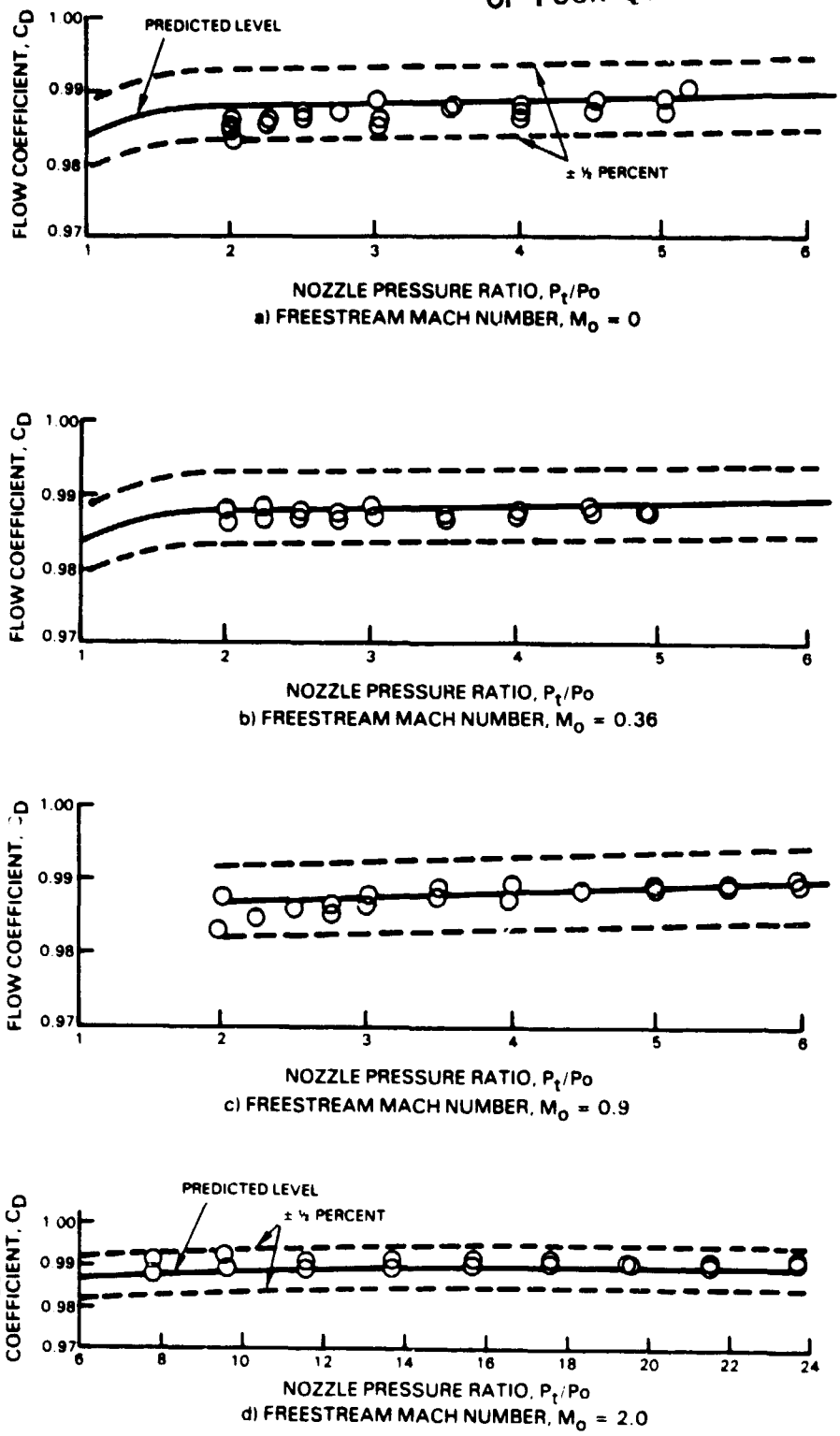

Figure A-3 Modified Supersonic Tunnel Association Nozzle Flow Coefficients

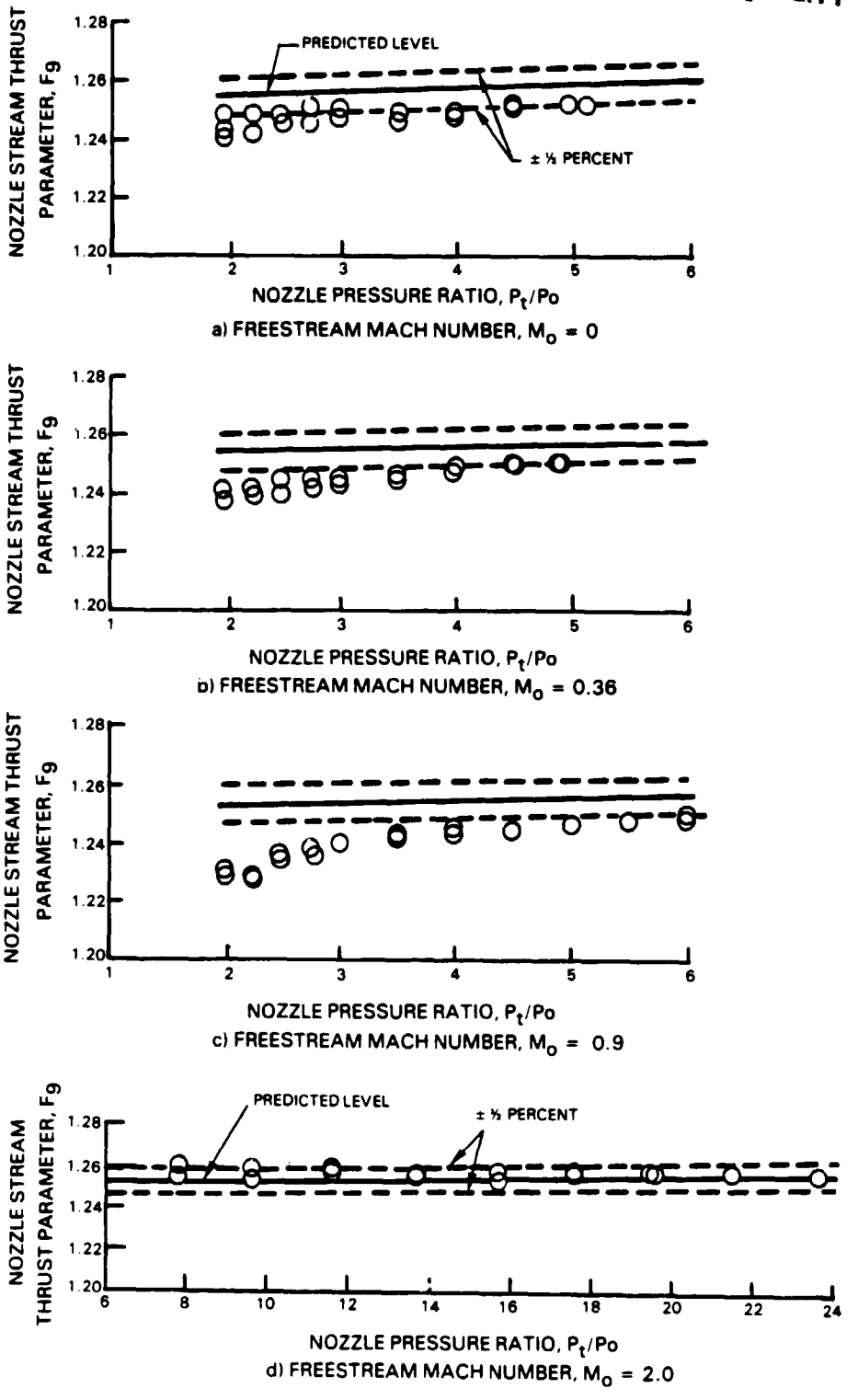

Figure A-4 Modified Supersonic Tunnel Association Nozzle Stream Thrust Parameters

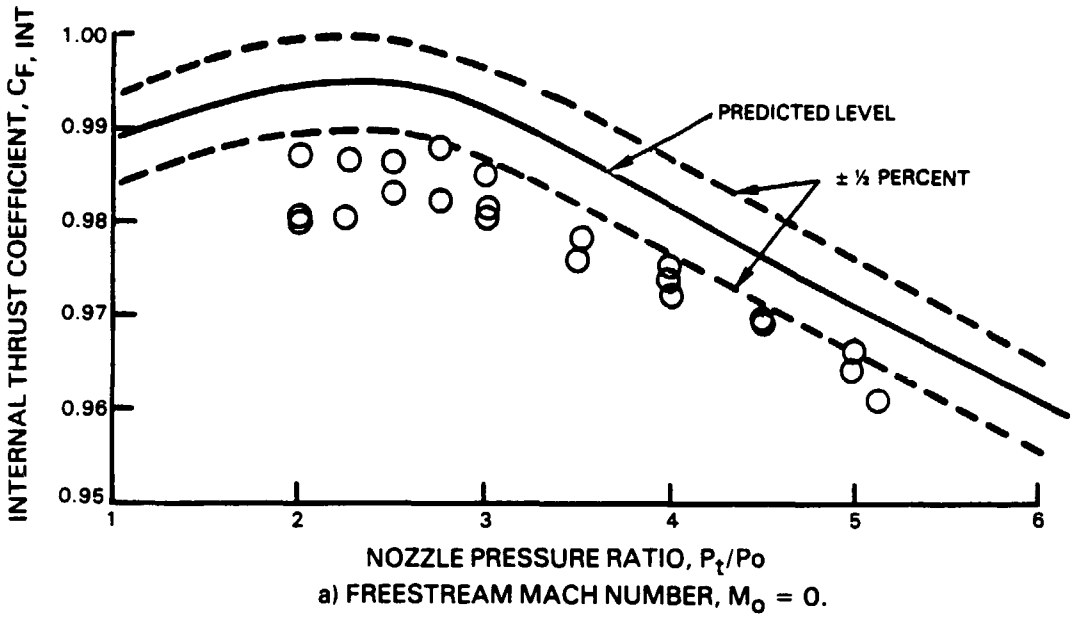

a) FREESTREAM MACH NUMBER, M_o = 0.

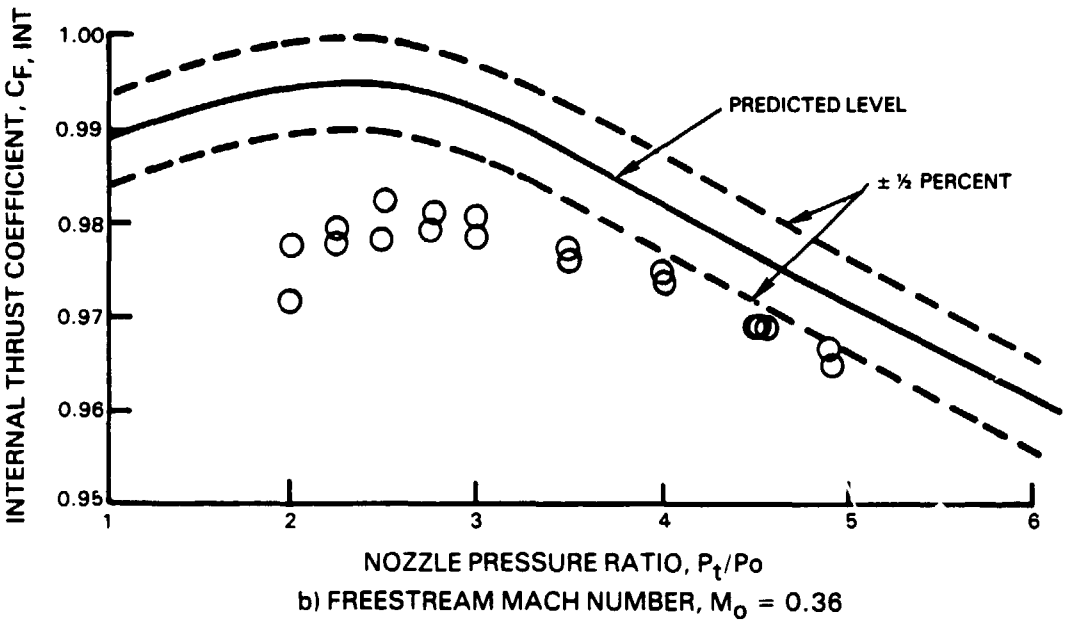

b) FREESTREAM MACH NUMBER, M_o = 0.36

Figure A-5 Modified Supersonic Tunnel Association Nozzle Internal Thrust Coefficients

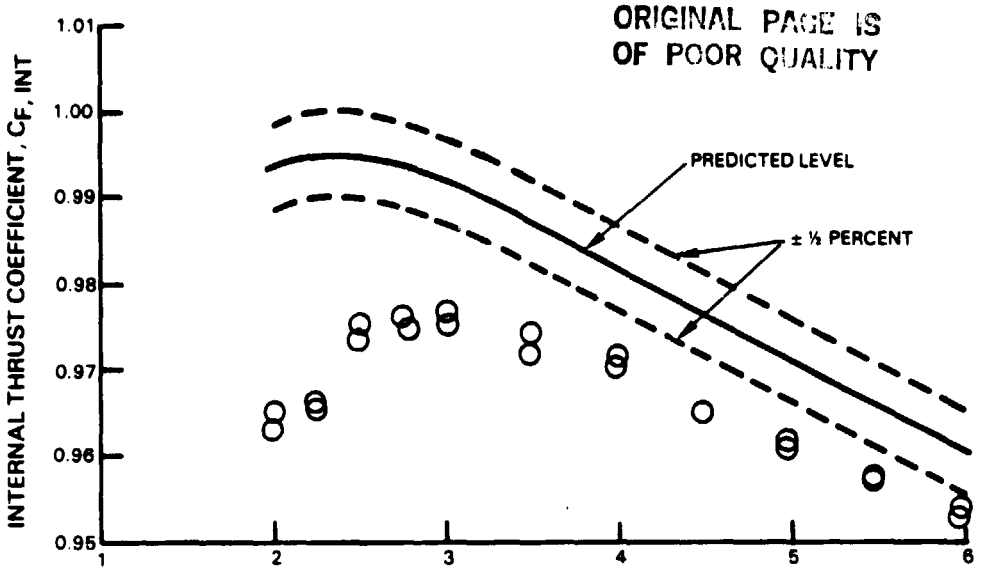

c) FREESTREAM MACH NUMBER, M_o = 0.9

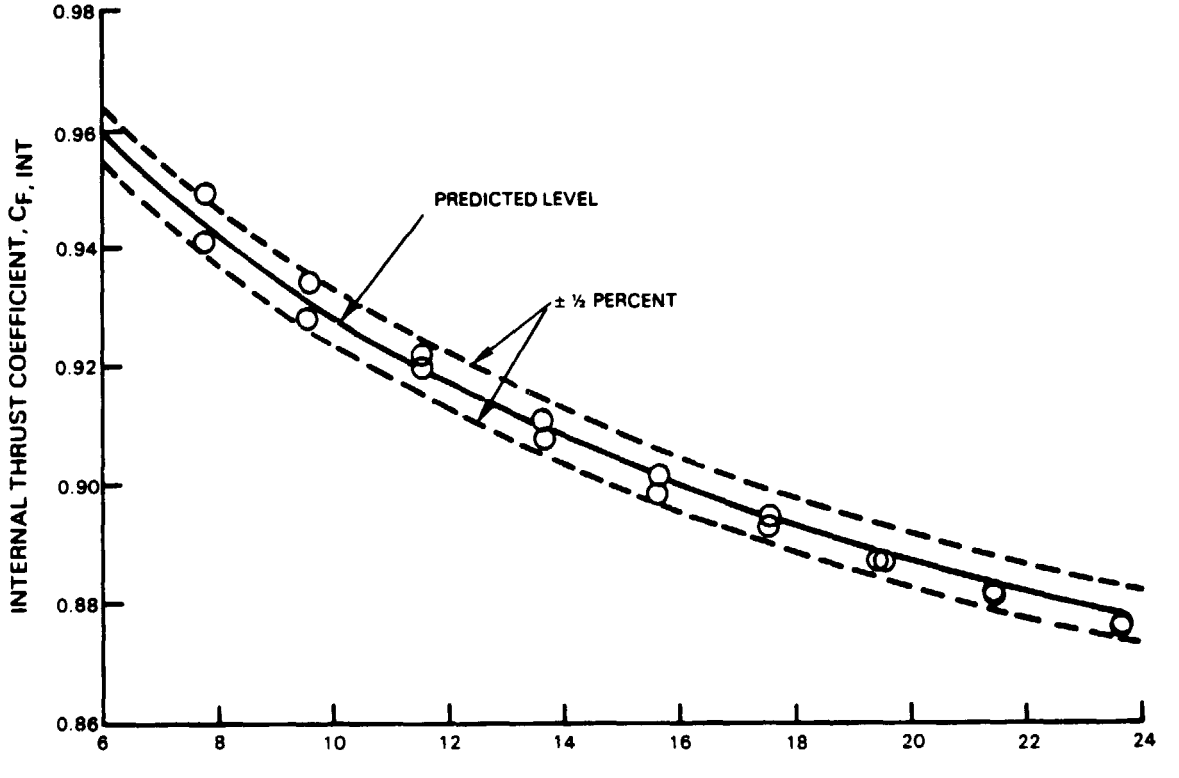

d) FREESTREAM MACH NUMBER, M_o = 2.0

Figure A-5 Modified Supersonic Tunnel Association Nozzle Internal Thrust Coefficients (Concluded)

APPENDIX B

LIST OF SYMBOLS

A	Area
B	Base
C	Constant relating venturi area ratio to one-dimensional pressure ratio
C-D	Convergent-divergent nozzle
C_D	Drag coefficient
C_d	Flow coefficient
Cf_{int}	Modified Supersonic Tunnel Association nozzle thrust coefficient
Cf	Thrust coefficient (not including external friction drag)
Cp	Pressure coefficient
D	Diameter, drag
F	Nozzle generated force, thrust
Fi	Nozzle ideal thrust
g	Gravitational constant
K	Compressibility correction
L	Length
m	Mass flow
M	Mach number
P	Pressure
q	Freestream dynamic pressure
R	Gas Constant
STA	Supersonic Tunnel Association
T	Temperature
V	Velocity
W	Weight flow
X	Axial distance
Y	Radial position

APPENDIX B

LIST OF SYMBOLS (Continued)

Greek Letters

α	Shroud internal divergence angle
β	Forebody boattail mean angle
γ	Specific heat ratio or plug angle
Δ	Difference of two terms
δ	Splitter trailing edge included angle
θ	Trailing edge flap boattail angle
ϕ	Circumferential position angle

Superscripts

*	Sonic flow condition

Subscripts

B	Base
ex	Exit
f	Fan duct
i	Ideal
inlet	Ejector inlet
int	Internal
j	Jet
l	Local
LC	Load cell
Max	Maximum
p	Primary duct
Ref	Reference cross-sectional area
s	Shroud
sm	Friction drag on metric portion of model
t	Total
v	Venturi

Numerals

0	Freestream or ambient condition